Melanesian back-arc basin and arc development: constraints from the eastern Coral Sea

Maria Seton[1*], Nick Mortimer[2], Simon Williams[1], Patrick Quilty[3], Phil Gans[4], Sebastien Meffre[3,5], Steven Micklethwaite[6a], Sabin Zahirovic[1], Jarrod Moore[1], Kara J. Matthews[1b]

[1]EarthByte Group, School of Geosciences, The University of Sydney, NSW 2006, Australia

[2]GNS Science, Private Bag 1930, Dunedin, 9054, New Zealand

[3]Discipline of Earth Sciences, University of Tasmania, Private Bag 79, Hobart, TAS, 7001, Australia

[4]Department of Earth Science, UC Santa Barbara, Santa Barbara, CA, 93106-9630, USA

[5]ARC Centre of Excellence in Ore Deposits, University of Tasmania, Private Bag 79, Hobart, TAS, 7001, Australia

[6]Centre for Exploration Targeting, University of Western Australia, Perth, 6009, Australia

[*] Corresponding author. e-mail: maria.seton@sydney.edu.au

[a] Present address: School of Earth, Atmosphere and Environment, Monash University, Melbourne, VIC, 3800, Australia

[b] Present address: Department of Earth Sciences, University of Oxford, South Parks Road, Oxford OX1 3AN, UK

Submitted to Gondwana Research

Abstract

The eastern Coral Sea is a poorly explored area at the north-eastern corner of the Australian Tectonic Plate, where interaction between the Pacific and Australian plate boundaries, and accretion of the world's largest submarine plateau - the Ontong Java Plateau - has resulted in a complex assemblage of back-arc basins, island arcs, continental plateaus and volcanic products. This study combines new and existing magnetic anomaly profiles, seafloor fabric from swath bathymetry data, Ar-Ar dating of E-MORB basalts, palaeontological dating of carbonate sediments, and plate modelling from the eastern Coral Sea. Our results constrain commencement of the opening of the Santa Cruz Basin and South Rennell Trough to c. 48 Ma and termination at 25-28 Ma. Simultaneous opening of the Melanesian Basin/Solomon Sea further north suggests that a single > 2,000 km long back-arc basin, with at least one triple junction existed landward of the Melanesian subduction zone from Eocene-Oligocene times. The cessation of spreading corresponds with a reorganization of the plate boundaries in the area and the proposed initial soft collision of the Ontong Java Plateau. The correlation between back-arc basin cessation and a widespread plate reorganization event suggests that back-arc basins may be used as markers for both local and global plate boundary changes.

Keywords

Eastern Coral Sea; Melanesia; SW Pacific; back-arc basin; subduction

1. Introduction

The Coral Sea lies in the north-eastern corner of the Australian Tectonic Plate, in a pivotal position at the juncture between two of the world's most tectonically complex regions: the SW Pacific and SE Asia (Fig. 1). While the origin and evolution of the western part of the Coral Sea, including the Queensland and Marion Plateaus and Coral Sea Basin is relatively well-known (Falvey and Taylor, 1974; Gaina et al., 1999; Weissel and Watts, 1979), the eastern Coral Sea, with its mosaic of ridges, plateaus and basins has a largely unknown history. Previous plate tectonic reconstructions seeking to explain the origin and evolution of the submarine features in the eastern Coral Sea have been limited. The area is either largely ignored in regional plate tectonic models (Hall, 2002; Sdrolias et al., 2003; Weissel and Watts, 1979), or overly simplified with inferred ages for many of the features (Schellart et al., 2006; Whattam et al., 2008; Yan and Kroenke, 1993). These poorly constrained models reflect the scarcity of marine geophysical data and geological samples from the area, the inherent complexity of the many ridges and basins, and substantial volcanic and tectonic overprinting. Such a significant gap in our understanding of the tectonic development of the Coral Sea is unsatisfactory particularly for an area that provides plate boundary continuity between the SW Pacific and SE Asia along the western Pacific boundary, and thus is critical for plate reconstructions of both areas. In addition, this area lies adjacent to the North Solomon subduction zone and Ontong Java Plateau, the site of a major plateau accretion and subduction event, which is believed to have occurred either in the Oligocene (Musgrave, 2013), Miocene (Petterson et al., 1999) or Pliocene (Cowley et al., 2004). This collision induced a subduction polarity reversal in the Pliocene (Cooper and Taylor, 1985). Understanding the evolution of the submarine features in the eastern Coral Sea may provide insights into the timing and processes of the Ontong Java Plateau collision and help identify the effects of a major collision event on the over-riding plate.

We present the results of a recent research voyage (SS2012_V06) on *RV Southern Surveyor* to the eastern Coral Sea in October-November, 2012 where 13,600 km^2 of swath bathymetry data, 6,200 km of magnetic and 6,800 km of gravity data were collected, together with igneous and sedimentary samples from 14 seafloor sites (Fig. 1). Swath bathymetry and magnetic anomaly data are used to model the timing and orientation of seafloor spreading in the Santa Cruz Basin. Geochemical analysis and Ar-Ar dating of recovered igneous samples together with paleontological age constraints from sedimentary samples at the dredge site locations are used to relate spreading in the Santa Cruz Basin to activity along the South Rennell Trough and the igneous activity along the Rennell Island Ridge. Combining the results of our study with recently dated dredge samples from earlier ORSTOM voyages (Mortimer et al., 2014), we develop plate tectonic reconstructions of the eastern Coral Sea since the Cretaceous underpinned by age constraints from both marine geophysical data and geological samples. Our plate reconstructions include a network of continuously closing plate boundaries (Gurnis et al., 2012), which can be used to provide plate boundary continuity between the SW Pacific and SE Asia during this time period.

2. Regional tectonic framework

The SW Pacific is characterised by a series of marginal basins, submerged continental slivers and back-arc—arc—forearc complexes largely controlled by the interaction of the Australian and Pacific Tectonic Plates since the Mesozoic (Crawford et al., 2003; Schellart et al., 2006; Sdrolias et al., 2003; Whattam et al., 2008; Yan and Kroenke, 1993) (Fig. 1). In contrast, SE Asia is an amalgamation of accretionary continental fragments, exotic terranes and intra-oceanic island arcs, formed largely from the long-term interaction between the Australian, Pacific and Eurasian plates and Gondwana-derived terrane accretion (Acharyya, 1998; Golonka, 2004; Hall, 2002; Metcalfe, 2009; Stampfli and Borel, 2002; Zahirovic et al.,

2014). These two tectonically complex regions are connected through the "Melanesian Borderlands" region, which includes the Coral and Solomon Seas.

The Coral Sea is bounded by the passive margin of eastern Australian in the west, the inactive Pocklington Trough and Papuan Peninsula to the north, the active South Solomon/San Cristobal and New Hebrides Trenches to the northeast and east, and the Lord Howe Rise/New Caledonia region to the south (Fig. 1). It consists of the relatively well-explored Coral Sea Basin and Queensland and Marion plateaus in the western part and a complex arrangement of poorly explored and under-sampled submarine plateaus, linear depressions, elongated ridges, oceanic basins and seamounts in the eastern part, including the Rennell Basin, Rennell Island Ridge, South Rennell Trough, West Torres Plateau and Santa Cruz and d'Entrecasteaux Basins (Fig. 1).

Many of the features in the area are named after Rennell Island, which lies in the eastern Coral Sea at 160°E, 11.5°S (Fig. 1). These include: the Rennell Island Ridge, East Rennell Island Ridge, Rennell Trough, Rennell Basin, South Rennell Trough and Rennell Fracture Zone (e.g. (Daniel et al., 1978; Landmesser et al., 1973; Larue et al., 1977)). As the region becomes better known, we consider this preponderance of the name 'Rennell' to be unhelpful in science communication, especially as some of these features are up to 700 km distant from Rennell Island. In this paper we retain the names South Rennell Trough and Rennell Basin as these are used by all aforementioned authors except Landmesser et al. (1973). Use of these names supersedes Rennell Fracture Zone and Rennell Trough, respectively. We also retain the name Rennell Island Ridge but restrict its use to the NW-SE striking part around Rennell Island. We rename the East Rennell Island Ridge of Landmesser et al. (1973) as East Lapérouse Rise (Fig. 3), and introduce the name West Lapérouse Rise, for a mirror image positive bathymetric feature on the western side of the South Rennell Trough, and separated

from Mellish Rise by a bathymetric low (Fig. 1). Lapérouse was the French navy officer and explorer whose expedition vanished in the Vanuatu area c. 1788 and was searched for by d'Entrecasteaux. Lapérouse probably would have transited from Australia to New Caledonia across this region. To our knowledge, Lapérouse has not previously been used as a name for an undersea feature. A further complication regarding feature names in the region is the use of Bellona Island and Bellona Plateau. Bellona Island lies to the north of Rennell Island (Fig. 2) at a latitude of ~11°S and is part of the Rennell and Bellona Province of the Solomon Islands. The Bellona Plateau is a largely submerged plateau located at the southern tip of the South Rennell Trough at a latitude of ~19°S.

Tectonically, the region is dominated by active subduction to the northeast and east, along the South Solomon/San Cristobal Trench and New Hebrides Trench (Fig. 1), with a minor amount (~20 mm/yr) of Pacific plate subduction along the North Solomon Trench (Tregoning et al., 1998) (Fig. 1). North of the Coral Sea, seafloor spreading is active in the Woodlark Basin.

The main bathymetric features in the eastern Coral Sea are described below and labelled in Fig. 1.

2.1. Louisiade Plateau, Louisiade Trough and Mellish Rise

The submerged Louisiade Plateau and Mellish Rise (Fig. 1) are inferred to be composed of continental material that rifted off the Australian margin during Tasman and Coral Sea opening in the Late Cretaceous-Paleocene (Gaina et al., 1998; Gaina et al., 1999; Willcox et al., 1980). Although no basement rocks have yet been recovered from either plateau, the similarity in seismic character to the Queensland and Kenn plateaus (Exon et al., 2006; Taylor and Falvey, 1977) and the recovery of sediments with terrigenous material from basement highs on the Mellish Rise (Hoffmann et al., 2008) strongly supports a continental

origin. In contrast, global compilations of Large Igneous Province (LIP) locations (Bryan and Ernst, 2008; Coffin et al., 2006) classify the Louisiade Plateau as an oceanic plateau implying that it is either entirely volcanic (Cowley et al., 1998) or capped by volcanics. The Louisiade Trough separates the Louisiade Plateau from the Mellish Rise and reaches depths of over 5500 m. It accommodated seafloor spreading during the opening of the Tasman and Coral seas, as evidenced by rift-related structures along the margins (Exon et al., 2006) and the identification of magnetic anomalies 27-26 (Gaina et al., 1999). No basement samples have been obtained from the Louisiade Trough.

2.2. Rennell Island Ridge and Basin

East of the Louisiade Plateau lies a short and narrow (50 km wide) depression with water depths exceeding 5000 m (Rennell Basin) (Figs 1, 3). Seismic reflection lines show a flat-floored basin partly filled with undeformed sediments and a trench-like morphology at the eastern margin (Récy et al., 1977). The undeformed sediments are believed to be Oligocene and younger (Récy et al., 1977). Previously-published models speculate that the Rennell Basin was the site of east-dipping subduction during the Eocene (Hall, 2002; Weissel and Watts, 1979; Yan and Kroenke, 1993) or the site of seafloor spreading (Landmesser et al., 1973), separating an inferred continental fragment, the Rennell Island Ridge, from the north-eastern margin of the Louisiade Plateau.

The Rennell Island Ridge is a ~200 km long and ~70 km wide largely submerged ridge structure east of the Rennell Basin (Fig. 1), with sub-aerial exposure of the Rennell and Bellona Islands and the shallow Indispensible Reef complex (Fig. 2). Rennell and Bellona Islands belong to the world's largest exposed raised coral atoll, consisting of a thick (up to 500 m) sequence of coral reefs and dolomite (Taylor, 1973) but with no basement exposures. Three alternative models for the origin of the Rennell Island Ridge have been

proposed. These include: an island arc above an east-dipping subduction zone with the Rennell Basin acting as the trench (Daniel et al., 1978; Weissel and Watts, 1979; Yan and Kroenke, 1993); a fragment of Mesozoic Australia-derived continental lithosphere with the Rennell Basin acting as an abandoned basin formed by seafloor spreading (Landmesser et al., 1973) and; oceanic basalt, similar in character to the Cretaceous uplifted oceanic crust found on the Malaita Islands in the southern Solomon Islands (Hughes and Turner, 1977). A basaltic dredge sample from the western margin of the Rennell Island Ridge revealed a geochemically depleted MORB- or arc-type rock with a minor degree of subduction-related geochemistry of 38 ± 5 Ma age (Mortimer et al., 2014). Deciphering the origin and evolution of the Rennell Island Ridge is further complicated by the substantial Quaternary uplift of the ridge linked to the proximal northeast-dipping subduction along the South Solomon Trench and Pliocene subduction polarity reversal.

2.3. South Rennell Trough

South Rennell Trough extends into the Santa Cruz Basin to the northeast, as observed in bathymetry and satellite gravity maps, and terminates at the Bellona Plateau in the southwest (Fig. 1 and 3). It is 700 km long, reaches depths of over 5000 m and includes a 30 km wide central trough and two prominent, parallel ridge systems. Previous models have proposed that the ridges and troughs formed either along a transform fault during the opening of the Tasman and Coral Seas (Landmesser et al., 1973), an extinct late Oligocene spreading ridge (Daniel et al., 1978; Larue et al., 1977), or a Cretaceous-Paleocene spreading ridge (Schellart et al., 2006). Recent geochemical analysis and Ar-Ar dating of basalt samples from the northern part of the South Rennell Trough (Mortimer et al., 2014) (Fig. 3) confirms MORB geochemistry of Oligocene age and hence, a spreading centre origin for the South Rennell Trough. Outstanding questions remain regarding the ridge features on either side of the

South Rennell Trough (the East and West Lapérouse Rises) (Fig. 3), and the relationship to the oceanic crust that formed in the Santa Cruz Basin.

2.4. Santa Cruz Basin

The Santa Cruz Basin is located in the corner of the eastern Coral Sea between the New Hebrides and South Solomon trenches and the West Torres Plateau and Rennell Island Ridge (Fig. 1). The size of the Santa Cruz Basin has been modified due to active subduction of the basin along the New Hebrides and South Solomon Trenches. Although there are no published magnetic anomaly interpretations of the basin, it is inferred floored by oceanic crust. However, the age of formation of the basin has been debated with models invoking either Cretaceous opening (Kroenke, 1984; Schellart et al., 2006), coincident with opening of the d'Entrecasteaux Basin to the south, or Oligocene opening (Larue et al., 1977; Wells, 1989; Yan and Kroenke, 1993) coincident with extension along the South Rennell Trough. Although recent analysis of dredges from the ORSTOM survey revealed 28 ± 1 Ma BABB type material from the Santa Cruz Basin (Mortimer et al., 2014) (Fig. 4), the spreading evolution of the basin has yet to be deciphered.

2.5. West Torres Plateau

The West Torres Plateau is a submarine plateau, located south of the Santa Cruz Basin and north of the d'Entrecasteaux Basin, which interacts with the New Hebrides Trench on its eastern border (Fig. 1). It has a depth range of ~1000-3500 m and a width of approximately 200 km (Fig. 5). The origin of the plateau is unknown, with no available dredge samples. Two alternative models exist for the nature of basement: a continental origin (Schellart et al., 2006), perhaps as a continental raft from eastern Gondwana, or a mantle plume origin, with the eruption of the associated LIP in the Oligocene (Yan and Kroenke, 1993). A continental origin for the West Torres Plateau would require an approximately east-

west spreading direction in the neighbouring d'Entrecasteaux Basin, unless significant north-south translation occurred subsequently. A LIP origin would require a connection to a past or present-day hotspot and the presence of an associated trail.

2.6. d'Entrecasteaux Basin

The d'Entrecasteaux Basin (sometimes referred to as the North d'Entrecasteaux Basin) is a fan-shaped basin bounded by the South Rennell Trough to the north, the arcuate-shaped d'Entrecasteaux Zone to the south, the West Torres Plateau to the east and the New Caledonia Basin and South Rennell Trough to the west (Fig. 1). A tentative interpretation based on limited magnetic anomaly profiles suggested a Cretaceous age (between anomalies 30-34; 65-84 Ma) (Lapouille, 1982) from roughly NW-SE directed spreading (Fig. 5). Although this interpretation has been questioned, no alternative interpretation of the magnetic lineations has been published and no in-situ samples have been collected. The relationship between the d'Entrecasteaux Basin and the surrounding area has been suggested in three ways: the d'Entrecasteaux Basin and North Loyalty Basin were originally one basin (Lapouille, 1982); the d'Entrecasteaux Basin, South Rennell Trough and Santa Cruz Basin share a common Cretaceous opening history (Schellart et al., 2006); and the d'Entrecasteaux Basin is the north-western extent of the New Caledonia Basin (Schellart et al., 2006).

The d'Entrecasteaux Basin terminates in the south at the d'Entrecasteaux Zone, a ~100 km wide arcuate structure consisting of various horsts and graben (Maillet et al., 1983) and partitioned into the North d'Entrecasteaux Ridge and the South d'Entrecasteaux Chain (see Mortimer et al. (2014) for description). Steep slopes mark its boundary into the North Loyalty Basin to the south and the West Santo and d'Entrecasteaux basins to the north (Fig. 5). Recent analysis and dating of samples from the North d'Entrecasteaux Ridge indicate primitive arc tholeiites of Eocene age. One sample yielded a 49 ± 10 Ma age for E-MORB

back-arc basin type rocks (Mortimer et al., 2014), although they caution that more samples need to be collected to confirm the interpretation.

3. Tectonic features and bathymetric interpretation

New swath bathymetry data were collected during the *SS2012_V06* research voyage using a 30 kHz Simrad EM300 multibeam echo sounder system (see Figs. S1-3). The data were processed using Caris software and were combined with regional, publicly available swath bathymetry data available through the NGDC, JAMSTEC and Geoscience Australia databases. Where swath coverage was unavailable, global bathymetry compilations were used. Seismic reflection profiles from the area (e.g. (Landmesser et al., 1973)) are typically old and crude but were useful to help reveal large-scale basement structure and faulting patterns.

3.1. Rennell Island Ridge and Rennell Basin

The Rennell Island Ridge is characterised by the sub-aerial exposure of Rennell and Bellona Islands and the shallow Indispensible Reef complex (Fig. 2). Regional bathymetry compilations and seismic reflection profiles (Landmesser et al., 1973) show thickened crust with variation in structure and morphology along strike. There are two main structural trends: a NW-SE orientation, similar to the south-western margin of the West Torres Plateau and parallel to Indispensible Reef and; a WNW-ESE orientation, similar to part of the trend of the South Solomon subduction zone and parallel to Rennell and Bellona Islands (Fig. 2). Between the two main structural trends in the southern part of the Rennell Island Ridge complex lies a small < 40 km wide, 1800 m deep trough with smooth seafloor (Fig. 2 and S1), which likely contains thick sediment accumulations that obscure the underlying smaller-scale structure. The Rennell Island Ridge is bounded by normal faults along its western margin (see Daniel et al. (1978) and Recy et al. (1977) where it rises from depths of over

3500 m at the edge of the slope to 1200 m at the shelf edge (Fig. 2). At its southern termination, the Rennell Island Ridge does not share structural affinities with the South Rennell Trough.

No available swath profiles exist across the Rennell Basin but previous seismic reflection lines show a flat-floored basin partly filled with undeformed sediments, the thickness of which increases southward (Daniel et al., 1978). In addition, seismic reflection profiles show a morphology and structure characteristic of an inactive subduction zone along the eastern margin (Daniel et al., 1978; Récy et al., 1977). However, this interpretation remains tentative and cannot be supported structurally without the addition of high-resolution bathymetry mapping from the Rennell Basin paired with the recovery of a suite of subduction-related rocks from the Rennell Island Ridge.

3.2. South Rennell Trough

Swath bathymetry profiles collected during *SS2012_V06* along the South Rennell Trough were combined with profiles from the *RV Melville* (BMRG07MV) and *RV Mirai* (MR0707) (Fig. 3). The South Rennell Trough is an extinct spreading centre, based on the E-MORB geochemistry and 28-29 Ma Ar-Ar dates of the recovered basalts from the edge of a rift graben (Mortimer et al., 2014). The broad scale structure is that of a deep (up to 5400 m), steep-sided (gradients up to 30°), wide (10-30 km) rift valley with a series of 2-3 sub-parallel abyssal hills/ridge lines on either side that become narrower southward as they transition in to the Bellona Plateau. These abyssal hills have elevations of between 1500-2000 m (highest along the outer ridge), giving a total relief, from rift valley to axial ridge, of ~3000-4000 m. The rift valley floor of the South Rennell Trough contains NE-SE-directed seafloor fabric (Fig. 3a). The similarity in trend between the abyssal hill fabric and the broad scale structure

of the ridge suggests no reactivation of the plate boundary after formation, as suggested by Coleman and Packham (1976)).

The morphology and structure of the South Rennell Trough share similar characteristics to the ultra-slow spreading Gakkel Ridge in the Arctic Ocean. The Gakkel Ridge is characterised by a deep axial valley (depth between 4700-5300 m), a width of ~15-30 km, a continuous ridge axis with no transform offsets and linear rift-parallel ridges, and fault-bounded troughs with up to 2000 m elevation (Cochran et al., 2003). In this scenario, the elevated ridges on either side of the South Rennell Trough, the East and West Lapérouse Rises, can be explained by the complex interplay between magma supply and plate stretching (Buck et al., 2005). The limits on seafloor spreading rates (maximum of 20 mm/yr; (Dick et al., 2003)) and the general morphology and structure of the South Rennell Trough complex can be used as a constraint on plate tectonic reconstructions of this seafloor spreading system.

3.3. Santa Cruz Basin

Three full and four partial swath profiles collected across the Santa Cruz Basin during voyage *SS2012_V06* were combined with a swath profile from voyage MGLN06MV on the *RV Melville* (Fig. 4 and Fig. S2).

The most pronounced feature in the Santa Cruz Basin is a wide (average width 20-30 km), >1000 m deep trough that is continuous with the South Rennell Trough (Fig. 4). Axial troughs of this depth and width are characteristic of slow (20-55 mm/yr) or ultra-slow (< 20 mm/yr) seafloor spreading where magma is supplied slowly enough for the crest of the ridge to subside as the oceanic plates cool. Faults on either side of the axial trough are numerous in slow spreading rifts and create typically rough topography, as is observed on either side of the axial trough in the Santa Cruz Basin (Fig. 4).

Away from the inferred extinct mid-ocean ridge, the swath data show clear abyssal hill fabric indicative of seafloor spreading. The abyssal hill relief is typically 100-300 m and rough, again suggesting a slow seafloor-spreading rate. The seafloor spreading fabric displays two main structural trends: 30° (from N) adjacent to the extinct ridge, similar to the fault trends in the South Rennell Trough; and a trend at 70° (from N) away from the extinct ridge in the east of the basin, beyond ~164° longitude (Fig. 4 and Fig. S2). This indicates a change from NNW-SSE oriented to NW-SE oriented spreading during the formation of the Santa Cruz Basin. Fracture zones were not identified in any of the profiles across the Santa Cruz Basin. The lack of fracture zones cannot be related to obstruction by sediment infilling as Luyendyk et al. (1974) and De Broin et al. (1977) described a subhorizontal, well-bedded sedimentary section less than 1 km thick in the basin. Instead, this may be related to the spreading rate, as ultra-slow and some slow spreading ridges characteristically lack transform segments (Dick et al., 2003).

Although the South Rennell Trough appears to extend into the Santa Cruz Basin, the elevated nature of the East and West Lapérouse Rises suddenly disappears at the point where the South Rennell Trough intersects the Rennell Island Ridge and West Torres Plateau (i.e., into the Santa Cruz Basin). This may reflect a difference in spreading processes, such as rate of seafloor spreading, between the South Rennell Trough (ultra-slow) and Santa Cruz Basin (slow to ultra-slow). However, the spatial relationship to the Rennell Island Ridge and West Torres Plateau suggests that there may be further differences, such as the initial rifting process or thermal structure.

3.4. West Torres Plateau

Two profiles were collected during the voyage *SS2012_V06* in a small section of the western margin of the West Torres Plateau (Fig. 5), which were combined with a swath profile from voyage KIWI10RR on the *RV Roger Revelle*.

The West Torres Plateau is steep-sided, oriented NW-SE, similar to the main structural trend of the Rennell Island Ridge (Fig. 2 and 5), and faulted along the southwestern margin (slopes greater than 30^{o}). Gentle slopes extend into the Santa Cruz Basin and New Hebrides Trench (Fig. 5). An arm of the West Torres Plateau protrudes westward near the South Rennell Trough. A detailed swath survey along this arm reveals N-S structural trends, which may be lava flow fields rather than reflecting underlying structural fabric (Fig. S1, C).

In the southwest corner of the West Torres Plateau lies a small basin, which has previously been included as part of the d'Entrecasteaux Basin. Two swath profiles that cross this basin from voyage KIWI10RR on the *RV Roger Revelle* and BMRG07MV on the *RV Melville* (Fig. 5) reveal NE-SW oriented seafloor fabric in the north, which changes to E-W oriented fabric in the south adjacent to the E-W trending features of the d'Entrecasteaux Zone. The fabric identified in these profiles confirms that this basin has a discrete opening history from the main part of the d'Entrecasteaux Basin.

3.5. d'Entrecasteaux Basin

Structural trends in both existing and newly collected swath bathymetry data reveal that the d'Entrecasteaux Basin consists of three discrete zones (Fig. 5). Zone 1 (Fig. 5) is the largest and forms the d'Entrecasteaux Basin proper. While three swath profiles collected during voyage *SS2012_V06* failed to yield useful structural information related to seafloor (Fig. S3), a swath profile that was collected adjacent to the South Rennell Trough by the *RV Mirai* during voyage MR0707 reveals NE-SW oriented structural trends in the basin (Fig. 5). Whether this fabric is indicative of seafloor fabric or late-stage faulting during South

Rennell Trough activity is unknown. Zone 2 (Fig. 5) is separated from the third by a narrow band of about 3000 m high seafloor. A single swath profile from voyage BMRG07MV on the *RV Melville* reveals roughly N-S oriented seafloor structures that may represent abyssal hill fabric (Fig. 5). TZone 3) is bounded by the West Torres Plateau to the north and east and the d'Entrecasteaux Zone to the south. In this basin, the structural trends are NE-SW oriented in the north, changing to E-W oriented in the south adjacent to the E-W trending features of the d'Entrecasteaux Zone (Fig. 5). The fabric to the north could be indicative of abyssal hill fabric with the E-W fabric likely related to later deformation along the d'Entrecasteaux Zone.

4. Rock samples

Samples described in this paper were obtained from seven dredge sites on the Rennell Island Ridge, West Torres Plateau, East Lapérouse Rise and the South Rennell Trough (Table 1 and Fig. S1 and S4). Rocks obtained from other dredge sites during voyage *SS2012_V06* comprise intra-plate lavas from the Lord Howe Seamount chain and the Zealandia continent and are presented in Morimer et al. (in review).

A subset of sorted dredge samples was given GNS Science "P numbers" and catalogued in GNS Science's National Petrology Reference Collection. Location, rock type and analytical data are lodged in the open file PETLAB database (http://pet.gns.cri.nz/result_list.jsp?Type=Ext&Collector=ECOSAT).

A range of volcanic and sedimentary rocks was dredged on voyage *SS2012_V06*, mainly basalts, limestones and calcareous mudstones. Summary rock type and age data are given in Table 1. Photographs of analysed rocks are shown in Fig. S4 with results plotted in Figs. 6-9 and S5. A detailed description of the methods undertaken can be found in the Supplementary Section with raw data given in the Supplementary Data tables.

4.1. Rennell Island Ridge

4.1.1. South-west side (DR2)

Only sedimentary rocks were recovered from this dredge site on the southwest side of Indispensable Reefs. Sample DR2C is a typical rock from this location. It consists of moderately hard olive green calcareous mudstone containing radiolaria and benthic foraminifera giving a late Early Miocene (N7/8) age. Most species groups have wide depth ranges but the low planktonic content and lack of diversity combined with diverse benthics suggests shelf conditions. Sample DR2E is a grey-cream bored mudstone containing a reasonable fauna of planktonic and benthic foraminifera of Middle Eocene (E10-12) age. Judging by the planktonic percentage and type of benthics present, deposition appears to have taken place in continental slope depths (200-2000 m). DR2H is a hard and bioturbated cream-grey mudstone with a prominent 1 cm thick graded sandy siltstone bed. On disaggregation, the mudstone yielded common radiolaria along with a few sponge spicules, echinoid spine fragments and low diversity foraminifera. The latter are of Middle-Late Eocene (E10-E15) age. Thin section contains some simple, large agglutinated benthic foraminifera (*Rhizammina/Hyperammina*). The benthic foraminifera in DR2E and DR2H are similar, suggesting the material is from the same, continental slope sequence.

The thin sandstone bed in DR2H is a heavy mineral layer consisting of detrital plagioclase, chlorite, titanomagnetite, ilmenite and chromite. No quartz, mica or zircon was present. Chromite chemistry indicates derivation from an eroding volcanic, rather than an exhumed peridotite, source (Fig. 7).

4.1.2. North-east side (DR3)

In contrast, at the DR3 dredge site on the northeast side of Indispensable Reefs, basalts were recovered along with sedimentary rocks. DR3C is a friable cream-coloured calcareous mudstone coating on the outside of basalt DR3Aiv. It consists dominantly of planktonic faunas of Middle Eocene (E13) and Quaternary (N22/23) age, deposited in a bathyal environment. DR3F comprises separate pieces of soft, friable muddy micritic limestone, not in physical contact with basalt. Excellent Middle Eocene (E11) planktonic fauna were obtained and also the deep-water benthic form *Nuttallides truempyi*. DR3H mainly comprises hard coral fragments; a non-coral piece of the sample contained foraminifera along with fragments of corals and bryozoans. The faunas are mixed and of Pliocene (N21) and Pleistocene (N22) age. Foraminifera types present are consistent with a shallower depth of deposition than the ooze samples of DR3C and DR3F.

The basalts from DR3 are mainly grey, sparsely plagioclase- and augite-porphyritic pillow lavas with glassy rinds (e.g., P82182). Some microdoleritic textured samples are present (e.g., P82183) and may be hypabyssal intrusions or the coarse interiors of lava flows. Chemical analyses reveal them to be similar, but not identical, subalkaline basalts. Multi-element normalised patterns (Fig. S5) show good coherency between incompatible element concentrations with P82182 being light rare-earth element (REE) enriched and heavy REE depleted with respect to P82183. P82182 is also more oceanic-island basalt-like than P82183. Nonetheless, both samples have compositions within the overall range of enriched mid-ocean ridge basalt (E-MORB).

Plagioclase from the same two basalts was dated by Ar-Ar methods. The gas release spectrum from P82182 plagioclase (Fig. 8A) is slightly U-shaped, but generally flat. K/Ca is low (0.002 to 0.005); radiogenic yields are 30-60% then drop. A pseudoplateau age based on the two steps at the bottom of the 'U' gives an age of 42.3 ± 1.2 Ma (2 sigma). This is

indistinguishable from an inverse isochron age of 41.6 ± 4.6 Ma based on the 750-1040°C steps (see Supplementary File). Plagioclase from the P82183 microdolerite has a similar, slightly U-shaped spectrum but higher K/Ca ratios (Fig. 8B). A weighted mean plateau age (WMPA) using 57% of the gas is 43.15 ± 1.0 Ma. This is within error of the isochron age of 43.5 ± 2.2 Ma using the same gas steps. Our preferred interpreted ages for P82182 and P82183 plagioclases are 42.0 ± 2.0 Ma and 43.2 ± 1.5 Ma, respectively. These are arrived at by rounding the plateau ages and by conservatively lowering the precision. A weighted average of these ages is 42.8 ± 1.2 Ma.

4.2. West Torres Plateau (DR4)

More than 99% of the dredge consisted of one rock type: amygdaloidal pillow basalt with glassy rinds and sparse, clay-altered olivine phenocrysts (e.g., P82188). Colour ranges from grey to dark orange depending on alteration. Amygdules are filled with calcite and chlorite. Some lavas are slightly more porphyritic with up to 10% clay-altered olivine phenocrysts (e.g., P82189). Manganese crusts and rinds up to 9 cm thick are present on all samples.

On the largest boulder some white, non-calcareous material forms matrix to hyaloclastite breccia and was subsampled as DR4Aiv. The few microfossils in it are dominantly in the form of chamber internal moulds. A few echinoid spines and coelenterate fragments are present. Only two identifiable specimens are noted. Both belong to the robust genus *Catapsydrax* also known to resist dissolution and diagenesis. If they are *C. stainforthi* then the sample is Early Miocene (N4-N7) but if they are *C. unicavus* then a broader, Late Eocene to Early Miocene (E13-N6) age range is indicated. Planktonic foraminifera in separate lumps of soft, pale brown ashy mudstone (DR4E) give a Quaternary (N22) age.

Glass from P82188 and holocrystalline whole rocks from P82188 and 82189 were analysed for whole rock geochemistry. We attribute the small compositional variation between glass

and whole rock (e.g., separation between the two red dots in Fig. 9) to element mobility in the slightly clay-altered whole rock. The DR4 West Torres Plateau samples are quite different from those at DR3 and have the overall geochemistry of subalkaline basalts from normal mid-ocean ridge basalt (N-MORB) suites. An N-MORB rather than arc-related origin for the DR4 samples is corroborated by the chrome spinel microphenocryst chemistry (Fig. 7).

Four magnetic splits of plagioclase and groundmass separates were made from P82189. Here we report the results for the analytically best (the least magnetic, most plagioclase-rich) fraction. The argon release spectrum climbs then flattens into broad plateau (Fig. 8C). K/Ca ratios are fair, as are radiogenic yields. As with the samples from DR3, the weighted mean plateau of 26.2 ± 0.8 Ma and inverse isochron age of 27.0 ± 1.7 Ma for the same gas release steps both agree within error. We report a preferred age of 26.2 ± 0.8 Ma for the eruption and cooling of this West Torres Plateau basalt.

4.3. East Lapérouse Rise

4.3.1. Northern part (DR5)

No igneous rocks were obtained from this dredge, which consisted of ~300 kg of limestones. DR5Aiii is a subsample of hard, cream-coloured recrystallised and cemented biocalcarenite. Thin section examination reveals common poorly preserved, thin-walled globigerinid planktonic foraminifera, lack of keeled globorotalids, and a sphaeroidinellid. Small benthic forms include miliolids and *Globocassidulina*. Large forms include *Amphistegina* (consistent with *A. hauerina*), and large, thin lepidocycline species. There are some echinoid spines.

DR5Av is another limestone subsample, of cavitated calcirudite containing broken coral clasts. A variety of planktonic and large (photic zone) foraminifera are present. Following Chaproniere (1984) an Oligocene-Early Miocene (N2-4) age estimate is based on the benthic

foraminifera *Lepidocyclina* (*Eulepidina*) ?*ephippioides, Heterostegina borneensis* and *Amphistegina hauerina.* The presence of *Miogypsinoides* in DR5Aiii reinforces the DR5Av age estimate and the presence of the sphaeroidinellid planktonic form in DR5Aiii suggests a Miocene rather than Oligocene age for the faunas. Planktonic ooze of Quaternary (N22) age is present on both DR5 samples.

4.3.2. Central part (DR6)

The only sample obtained from this dredge is a single Mn crusted cobble of orange-grey plagioclase- and olivine-porphyritic basalt (P82193). A 5-10 mm thick glass rind adheres to one side of the rock. The glass has the geochemistry of a typical E-MORB (Fig. 9). This is supported by the chrome spinel microphenocryst chemistry that straddles the MORB and OIB fields (Fig. 7).

Plagioclase from P82193 gives an excellent flat argon release spectrum although K/Ca ratios are very low (Fig. 8D). Radiogenic yields are good for most of the spectrum (60-88%). With the well-defined plateau and isochron, the biggest uncertainty stems from large Ca corrections. The WMPA (92% of gas) yields 39.3 ± 0.6 Ma and inverse isochron age of 39.1 ± 1.2 Ma. Conservatively, we choose the isochron age to be representative of the cooling and eruption of this basalt lava.

4.4. South Rennell Trough

4.4.1. West scarp (DR13)

A moderate quantity of limestone was obtained from the dredge, but no other rock types. A hard, bored, pale, cream-coloured foram limestone with a 5 mm think manganese oxide rind, lacking corals or shell fragments, (DR13Ai) was chosen for micropaleontological study. The disaggregated residue consists of planktonic foraminifera ooze. The moderately diverse

species indicate a late Middle to middle Late Miocene age (N14-N17A) and a -deep-water environment.

4.4.2. East Scarp 'Ski Jump' (DR14)

More than 99% of this dredge consisted of basalts and associated volcaniclastic breccia, sandstone and mudstone. Some slabs of the finer grained sedimentary lithologies were studied to try and date the volcaniclastic rocks. DR14Ai is a yellow-brown calcareous volcaniclastic mudstone, penetrated by manganese oxide nuclei and stringers. Sponge spicules, radiolaria, diatoms, echinoid spines, minute bivalves and ostracods are present. Planktonic foraminifera are quite common and are dominated by large simple globigerinid species. They are of Pliocene (N19-21) age. The diversity of accompanying invertebrates suggests moderately shallow water but this is normally in conflict with the presence of radiolaria.

Of the many individual basalt samples recovered from this 400 kg dredge, at least 15 separate volcanic lithotypes were identified on the basis of phenocryst content and grain size. Geochemical analyses were made of five representative samples: P82204 is a dark grey to orange olivine-phyric basalt with a glassy rind, P82206 is a non-glassy basalt with 15% clay-altered olivine phenocrysts, P82212 is an aphyric basalt, P82214 is a highly amygdaloidal (c. 30%) basalt and P82217 is a possible olivine-, augite and plagioclase-phyric basalt.

Geochemically, P82206 and 82214 are picritic (>12 wt% MgO and >180 ppm Ni). However, these two are not more depleted in any trace elements than the other three and, together, all five samples appear to be from the same igneous suite. Element ratios and concentrations seem typical of E-MORB compositions and transitional to ocean island basalt (OIB) (Fig. 9). Chrome spinel compositions from P82206 (DR14Eiii) are also transitional between these lava types (Fig. 7).

Two of the basalts were selected for dating. P82206 was fresh and unaltered enough for groundmass to be selected (the only groundmass dated in this sample set). It has a moderately flat argon release spectrum. Ages monotonically decrease during the first 75% indicating recoil in this part of the spectrum, K/Ca ratios are reasonably high (0.02 to 0.9), but radiogenic yields are very low (12-25%). Three steps (670-770°C) yield a small weighted pseudoplateau of age 30.1 ± 0.5 Ma with an accompanying isochron age of 30.8 ± 1.6 Ma. However, given the fine grain size of the groundmass and the clear evidence for recoil makes us wary of over interpreting it. Our preferred age is 30.0 ± 2.0 Ma, a combination of the central age with decreased precision.

Plagioclase from basalt P82217 gave an excellent flat spectrum, with reasonable K/Ca ratios (0.005 to 0.063) and radiogenic yields (60-95%). Analytically, this was one the highest quality samples in our dataset. Weighted mean plateau and isochron ages are both well defined at 34.7 ± 0.4 Ma (79% of gas) and 34.3 ± 1.2 Ma (100% of gas), respectively (Fig. 8F). Our preferred interpreted age for eruption and cooling of this lava is the weighted mean plateau age with a slightly decreased precision, namely 34.7 ± 0.5 Ma.

5. Magnetic anomaly interpretation

Much of the eastern Coral Sea suffers from a paucity of magnetic anomaly profiles. During voyage *SS2012_V06*, a total of 6,200 km of magnetic anomaly data were collected using a SeaSPY high sensitivity total field magnetometer. Profiles focused in the Santa Cruz and d'Entrecasteaux Basins. These data were combined into an in-house ship track marine geophysical database maintained at the University of Sydney (primarily contains data from the NGDC (National Geophysical Data Centre) database) and compared to the geomagnetic reversal timescale. The structural interpretation, in particular the abyssal hill fabric imaged by swath profiles, was used to guide the orientation and direction of spreading. We

interpreted a sequence of magnetic anomalies using the timescale of Gee and Kent (2007), and created a set of magnetic anomaly identifications using the picking convention as described in Seton et al. (2014). The magnetic anomaly identifications were used as the primary constraint in developing a tectonic history (and associated tectonic rotation parameters) for basin opening.

5.1. Santa Cruz Basin

Previous estimates of the age of the oceanic lithosphere within the Santa Cruz Basin have ranged from Cretaceous (Kroenke, 1984; Schellart et al., 2006) to Eocene-Oligocene (Larue et al., 1977; Mortimer et al., 2014; Wells, 1989; Yan and Kroenke, 1993) (see Section 2). Recent dating of E-MORB samples from the South Rennell Trough and Santa Cruz Basin (Mortimer et al., 2014) supports the Oligocene interpretation. However, no attempt has been made to interpret the magnetic anomaly data in the Santa Cruz Basin to place constraints on the basin evolution.

We collected three full and four partial profiles over the Santa Cruz Basin during voyage *SS2012_V06* to supplement existing magnetic data (Fig. 10). We identify magnetic anomalies 13o-20o (33.5-43.8 Ma) in the Santa Cruz Basin (Fig. 10 and 11), with younger anomalies present close to the ridge crest and potentially older anomalies in the northwest corner of the basin, perhaps up to anomaly 21o (47.9 Ma). Our interpretation is consistent with the age constraints provided by the dated dredge samples from the area (see Section 4 and Mortimer et al. (2014)). The seafloor-spreading direction, as inferred from tracing the magnetic anomalies between profiles, is ESE-WNW close to the ridge, consistent with the abyssal hill trends identified in the swath bathymetry data. The change in spreading direction is dated to ~36-35 Ma. We model three changes in spreading rate during the opening of the Santa Cruz Basin, with a slow rate of approximately 45 mm/yr during the initial stages of seafloor

spreading from anomalies 20o-18o (43.8-40.1 Ma) and a decrease to 30 mm/yr from anomalies 18o-13y (40.1-33.1 Ma) (Fig. 11). Close to the ridge, where the identification of magnetic anomalies is problematic, we model a further decrease in seafloor-spreading rate to around 10 mm/yr, in line with estimates along ultra-slow seafloor-spreading ridges (Dick et al., 2003).

While no fracture zones were identified in the swath bathymetry or gravity anomalies, the abyssal hill fabric observed in the swath data and the correlation of the magnetic anomalies across profiles leads us confidently to interpret the spreading direction as being predominantly NW-SE directed.

The timing of spreading cessation in the Santa Cruz Basin inferred from the magnetic anomaly data is difficult to quantify. Approximately 30-40 km of crust exists between the youngest identified anomaly and the axial ridge of the mid-ocean ridge (clearly identified in swath data). The difficulty in interpreting the data here may reflect a combination of a decrease in seafloor spreading rate to ultra-slow and increasing tectonic and magmatic complexity during final stages of seafloor spreading. Reducing the seafloor-spreading rate to around 10 mm/yr predicts a minimum date for cessation of spreading in the Santa Cruz Basin to 28-29 Ma, consistent with the basalt ages (28 Ma, (Mortimer et al., 2014)) from the crest of the South Rennell Trough. However, as spreading may have waned for several million years, we infer that 28 Ma is the minimum time of spreading cessation.

The initiation of seafloor-spreading in the basin is also difficult to determine because much of the northwestern flank of the basin and a portion of the eastern flank have been lost to subduction. The oldest confidently identified magnetic anomaly is 20o (43.8 Ma) but there is the potential for anomaly 21o (47.9 Ma) in the northwest. One limiting factor on the age of initiation of spreading in the Santa Cruz Basin may be whether or not space is available

between the oldest mag netic anomaly on the south-eastern flank and the West Torres Plateau to accommodate anomaly 21o. With this consideration and an assumption of slow spreading rates, we assume that the initiation of spreading could have occurred from around 48 Ma or slightly earlier. However, this is only a valid constraint if the West Torres Plateau was a pre-existing feature and not erupted on top of older seafloor. If the West Torres Plateau is confirmed to be a volcanic feature that formed after or during the opening of the Santa Cruz Basin, then the maximum age of formation for the Santa Cruz Basin can be extended by an additional 4-5 million years.

Our interpretation of the magnetic data from the Santa Cruz Basin confirms an Eocene-Oligocene age for the basin with the inferred spreading centre a continuation of the South Rennell Trough. This is in agreement with a recent reinterpretation and age dating of several ORSTOM samples from the South Rennell Trough as Eocene-Oligocene (Mortimer et al., 2014).

5.2. d'Entrecasteaux Basin

The existing magnetic anomaly profiles in the d'Entrecasteaux Basin have been used to interpret the basin as having formed in the Cretaceous (83-65 Ma; anomalies 30-34) with three different spreading orientations: E-W, NE-SW and WNW-ESE (Lapouille, 1982) (Fig. 12). According to Lapouille (1982), the d'Entrecasteaux Basin has a shared spreading history with the North Loyalty Basin to the south, separated by the d'Entrecasteaux Zone after the cessation of seafloor-spreading. Other studies have instead suggested a shared Cretaceous spreading history between the d'Entrecasteaux and Santa Cruz Basins (Kroenke, 1984; Schellart et al., 2006).

We collected four profiles across the d'Entrecasteaux Basin during voyage *SS2012_V06* to supplement existing magnetic data (Fig. 12). An interpretation of the age of the basin via

magnetic anomalies remains difficult due to the lack of magnetic anomaly pattern continuity between profiles (Fig. 12). However, a combination of structural data from the basin, integrated with new seafloor-spreading interpretations and age-dating from the surrounding areas allows us to discount several previous scenarios for basin formation.

Firstly, the prevailing interpretation of Lapouille (1982) (Fig. 12) can no longer be used to date basin opening as the magnetic lineations cross-cut the structural trends from the three zones that make up the d'Entrecasteaux Basin (Fig. 5 and 12). The N-S and NE-SW structural trends cover the area interpreted by Lapouille (1982) as having formed via NW-SE and ENE-WSW spreading. In addition, anomaly 34 of Lapouille (1982) cross-cuts the South Rennell Trough where a clear NW-SE spreading direction and Oligocene opening age has been established (see previous section).

Secondly, the Santa Cruz Basin and d'Entrecasteaux Basin cannot share the same Cretaceous opening history, as suggested by Kroenke (1984) and Schellart et al. (2006). A Cretaceous opening history would require that the age of the Santa Cruz Basin is also Cretaceous but this basin has unequivocally been dated to Eocene-Miocene with a shared spreading history along the South Rennell Tough (Mortimer et al., 2014). An alternative possibility that the d'Entrecasteaux and Santa Cruz basins still shared a common spreading history but during the Eocene-Oligocene, with the d'Entrecasteaux Basin reflecting one flank of the oldest portion of the South Rennell Trough, can also be discounted as this interpretation would require that oceanic crust of equivalent extent was present to the west of the West Lapérouse Rise (assuming spreading symmetry) or that a period of short-lived subduction occurred close to it. There is no geological or geophysical evidence to suggest either scenario is possible.

Thirdly, the d'Entrecasteaux Basin and the North Loyalty Basin cannot have a shared spreading history, as suggested by Lapouille (1982), as the structural trend in the

d'Entrecasteaux Basin , which lies adjacent to the North Loyalty Basin is almost perpendicular. Age dates from along the d'Entrecasteaux Zone, which range from ~50 to 30 Ma (Mortimer et al., 2014) indicate that there was a tectonic boundary between these two basins during the opening of the North Loyalty Basin (Sdrolias et al., 2003).

6. Discussion

6.1. Opening history of the South Rennell Trough and Santa Cruz Basin

Combining the petrological and microfossil analyses of dredge samples, structural interpretation of the region and magnetic anomaly interpretation of the Santa Cruz Basin, we create a rotation model for the opening of the South Rennell Trough and Santa Cruz Basin as a single spreading system (Fig. 13). Our finite rotations for the opening of the Santa Cruz Basin and South Rennell Trough, computed using the visual-fitting technique (i.e. manual-fitting of data) in the plate reconstruction software, *GPlates* (Boyden et al., 2011), can be found in the Supplementary Data.

We model the initiation of basin opening to have begun at 48 Ma in the Santa Cruz Basin based on the possibility of magnetic anomaly 21o being present in the northwest of the Santa Cruz Basin, with southward propagation occurring along the South Rennell Trough. The agreement in ages of the independently-dated volcanic and sedimentary rocks at site DR3 on the south-eastern edge of the Rennell Island Ridge lends strong support to the idea that the age of formation of igneous crust at these sites is at least middle Eocene. A middle Eocene age for the East Lapérouse Rise (DR6) and a late Eocene to early Oligocene age for the southern end of the South Rennell Trough is also clear from the data and consistent with the magnetic anomaly data for basin opening from the Santa Cruz Basin.

The southward propagating ridge stops in the south where it intersects with the Bellona Plateau, along the Lord Howe Seamount chain (one of several southward-younging hotspot trails in the SW Pacific). The pole of rotation for the initial opening was centred near the Bellona Plateau at 17.52°S, 158.63°E and migrated to 17.18°S, 158.82°E at the time of spreading cessation. As such, seafloor spreading rates vary quite significantly along strike from between 30-45 mm/yr in the Santa Cruz Basin to 10-30 mm/yr in the southern part of the South Rennell Trough during the main period of basin opening. This results in a characteristic fan-shaped basin opening pattern.

Cessation of seafloor spreading is primarily constrained from the dating of MORB at the ridge crest at 28 Ma (Mortimer et al., 2014) and is also consistent with the magnetic anomaly interpretation in the Santa Cruz Basin (see Section 5.1). Spreading rates may have decreased to as low as 10 mm/yr in the Santa Cruz Basin at around this time, consistent with typical <12 mm/yr rates for other ultra-slow spreading systems (Dick et al., 2003). Ultra-slow spreading systems report E-MORB glass compositions from these ridge axes (e.g. Mühe et al. (1997)), similar to the compositions we report, further supporting an ultra-slow spreading regime. However, it is important to note that a wider range of N-MORB and K-rich compositions have also been sampled in ultra-slow spreading regimes (Michael et al., 2003; Nauret et al., 2011). The final timing of cessation of basin opening can be constrained at 28 Ma as a minimum age, but may have waned for several million years until the complete depletion of the magma supply. We therefore suggest an age range for basin cessation between ~28-25 Ma. Other ultra-slow spreading systems also exhibit a gradual decrease in spreading rate until final termination of spreading (e.g. Labrador Sea (Delescluse et al., 2015)).

Our model for the South Rennell-Santa Cruz spreading system is of an ultra-slow, back-arc spreading system. We infer this spreading to have taken place in a back-arc basin setting because, although exact SW Pacific Paleogene paleogeography is speculative, arc-related igneous rocks of Eocene age have been reported from more Pacific-ward positions than the South Rennell Trough. These include the d'Entrecasteaux Ridge (Mortimer et al., 2014), New Caledonia (Cluzel et al., 2006), Fiji (Todd et al., 2012), Vanuatu (Buys et al., 2014) and the Tonga forearc (Meffre et al., 2012).

Compositionally, all lavas thus far sampled (at five sites) in and around the South Rennell Trough spreading system are distinctly E-MORB-like (Fig. 9). These plot further along the mantle array towards OIB than any lavas from other SW Pacific back-arc basins including the South Fiji, North Loyalty and Coral Sea basins. The possible Lord Howe plume influence on the South Rennell Trough lavas is explored in a companion paper (see Williams et al. (2014)). Alternatively, E-MORBs may be indicative of an Indian mantle-derived MORB source rather than Pacific mantle, an explanation used by Mortimer et al. (2012) for Tasman Sea Basin MORBs. Whatever the explanation, the E-MORB lava types of the South Rennell Trough do seem geographically unique.

An intriguing aspect of the South Rennell-Santa Cruz spreading system is the nature of the elevated and bathymetrically symmetrical East and West Lapérouse Rises. These rises are modelled to be the magmatic footprints of an ultra-slow spreading ridge and may be analogous to the magmatic or amagmatic ridge structures, a key component of ultra-slow spreading systems, as reported by Dick et al. (2003). In our model for basin opening, we assume that the East and West Lapérouse Rises were formed during the opening of the South Rennell Trough rather than being pre-existing ridge features that rifted apart with the establishment of the South Rennell spreading ridge. This does not preclude that some

inherited continental or other older volcanic material may have been isolated during the initial stages of basin opening.

6.2. Tectonic evolution of the eastern Coral Sea

The tectonic evolution of the eastern Coral Sea encompasses the history of the Melanesian and New Hebrides Arcs, the northeast Australian and Papuan margins and the tectonic processes occurring north of New Caledonia. We develop our plate tectonic model within the context of the results presented in this paper, recognising that there are many alternative models for the wider SW Pacific and SE Asian region. Our model is merged with the global plate tectonic model of Müller et al. (2016) with modifications in Zahirovic et al. (in review).

We initiate our model at 85 Ma (late Cretaceous), where we firstly consider the characteristics of the eastern Gondwana margin, which form the western and southern passive margins of the present-day eastern Coral Sea and provide a basis for interpreting material dispersed throughout the SW Pacific.

6.2.1. Late Cretaceous-Paleocene

A series of recent studies on the island arcs of the SW Pacific have identified continental-derived zircons from the Australian margin sitting within the island arcs of the Tonga Arc (Falloon et al., 2014), Vanuatu (Buys et al., 2014) and the Solomon Islands (Tapster et al., 2014) suggesting that many of these island arcs may have origins from Gondwana rather than being purely intra-oceanic in nature. The Melanesian Arc, for example, has previously been modelled as an intra-oceanic arc formed by spontaneous subduction initiation sometime in the Paleocene (e.g. Gaina and Müller (2007); (Hall, 2002); Yan and Kroenke (1993)), which conflicts with the new evidence from Tapster et al. (2014) and may support the model for subduction initiation at relic island arcs proposed by Leng and Gurnis (2015). Although

recognised, the timing for rifting of these fragments from the Gondwana margin remains unconstrained. In our model, we follow a simple scenario whereby portions of the Melanesian and New Hebrides Arc (Vanuatu) rifted from the Gondwana margin (adjacent to present-day Queensland, see Buys et al. (2014)) during the Cretaceous (Fig. 14A-B). We model this rifting phase to be contemporaneous with a major change in the tectonic regime along eastern Gondwana in the Cretaceous, which eventually led to the dispersal of continental blocks and the subsequent opening of the Tasman and Coral Seas (Gaina et al., 1998; Gaina et al., 1999) (Fig. 14C). We follow the model of Gaina et al. (1998) for the opening of the Tasman Sea at 90 Ma (late Cretaceous) and Gaina et al. (1999) for the opening of the Coral Seas and Louisiade Trough (and initiation of the Australian-Lord Howe-Louisiade triple junction) at 61 Ma (Early Paleocene). Our model additionally includes the contemporaneous opening of a series of back-arc basins oceanward of the Tasman and Coral Seas, such as the South Loyalty Basin adjacent to the Lord Howe Rise (Cluzel et al., 2001), according to the model of Matthews et al. (2015), and a new model for the opening of the newly named Emo Basin adjacent to the Coral Sea and PNG (Fig. 14B).

Our model for the Emo Basin is based on trace element, rare earth element and isotopic signatures of the Emo Metamorphics (part of the Owen Stanley Metamorphic Belt, Papuan Peninsula) that indicate tholeiitic influence with normal mid-ocean ridge basalt and enriched mid-ocean ridge basalt compositions that formed in a back-arc setting (Worthing and Crawford, 1996). While the age of the Emo Metamorphics is poorly constrained, Maastrichtian (~71-65 Ma) aged foraminifera are found in carbonate lenses within the structurally equivalent Goropu Metabasalt (part of the Milne Terrain) suggesting that the Emo Metamorphics protolith likely existed at this time (Smith and Davies, 1976; Worthing and Crawford, 1996). A Maastrichtian age is also proposed for crystallisation of the Papuan Ultramafic Belt (PUB) Ophiolite based on dating of foraminifera found in sediments

intercalated in the basalts (Belford, 1976; Smith and Davies, 1976), suggesting that the basin that formed the underlying crust is at least this old. The Late Cretaceous crystallisation age of the supra-subduction oceanic crust that forms the ophiolites is consistent with our interpreted age of north-dipping subduction initiation along the Sepik Arc to consume the latest Jurassic to Early Cretaceous Sepik Basin (Zahirovic et al., in review). The Sepik composite terrane is interpreted to be a composite terrane with continental and intra-oceanic crust, which is separated from New Guinea by the Central Ophiolite Belt, and separated from the younger (South) Caroline Arc to the north by the strike-slip faults that make up the Papuan Mobile Belt, following the terminology of Hall (2002) and Zahirovic et al. (2014). Lus et al. (2004) dated hornblende samples from the metamorphic sole of the PUB to determine the timing of cooling of the sole, and obtained a mean age of 58.3 ± 0.4 Ma using $^{40}Ar/^{39}Ar$ dating, providing a minimum age of formation of the Emo Basin. The Milne Terrain, to the southeast of the PUB, consists of upper Cretaceous and Eocene rocks of MORB-type affinity (Smith, 2013). Although these ages are consistent with those of the Emo Metamorphics, Smith (2013) argued that geochemical data indicate that the Milne Terrain formed by the opening of the Coral Sea Basin rather than a back-arc basin such as those of the Emo Metamorphics.

We model the opening of the Emo Basin to occur from 85 Ma (late Cretaceous), coincident with the opening of the South Loyalty Basin further south (Matthews et al., 2015). The obduction of the Emo Metamorphics and Papuan Ultramafic Belt are modelled to occur at 58 Ma (late Paleocene), induced by the opening of the Coral Sea basin at 61 Ma (Fig. 14C). As these back-arc basins opened, elements of the Melanesian and New Hebrides Arc were isolated from the Gondwana margin (Fig. 14A-B).

Previous models suggest southward-dipping subduction along the Melanesian and New Hebrides Arcs and Fiji, which together formed the Vitiaz Arc in the Eocene, with a

connection to the proto-Tonga-Kermadec Ridge further south (Gaina and Müller, 2007; Hall, 2002; Schellart et al., 2006; Sdrolias et al., 2003; Yan and Kroenke, 1993). The presence of arc-related volcanism from the Melanesian Arc (Jajao Igenous Suite on Malaita and Santa Isabel islands, Solomon Islands) between ~62-46 Ma (Tejada et al., 1996), evidence for late Eocene volcanism in New Britain (Lindley, 1988) and subsequent U-Pb dating of this volcanism (Holm et al., 2013), Ar-Ar and U-Pb dating of arc-rocks from Vanuatu indicating late Eocene-Miocene arc volcanism (Buys et al., 2014), and Eocene to early Miocene arc-volcanism in Fiji (see Taylor et al. (2000) for references) all support subduction occurring along this arc system at this time. In addition, the supra-subduction zone nature of the Jajao Igneous Suite (similar to BABB) may constrain the timing for back-arc basin formation behind the Melanesian Arc (Tejada et al., 1996). Although limited arc-related rocks exists that record active subduction prior to the Eocene, our model predicts that southward-dipping subduction along this arc system has occurred since at least the Late Cretaceous (Fig. 14), with a likely increase in subduction roll-back after the initiation of seafloor spreading in the Coral Sea at 61 Ma (Gaina et al., 1999), cessation of spreading in the Emo Basin and the initiation of its closure. Extending the subduction record back to the Cretaceous is based on a combination of the Late Cretaceous-aged arc rocks of the Jajao Igneous Suite (Tejada et al., 1996); ages and interpretations of South Loyalty Basin crust obducted onto New Caledonia based on the extensive review of Matthews et al. (2015), which supports Cretaceous subduction along eastern Gondwana; and plate kinematic and geodynamic considerations such as the requirement of a subduction zone to drive back-arc opening in the Emo Basin. The phase of arc volcanism recorded in the rocks from the Vitiaz Arc system from the Eocene may reflect the plate boundary readjustments that would have occurred synchronous with these events. After the initiation of Emo Basin closure, we model an oceanward jump in the location of back-arc basin opening behind the Melanesian portion of Vitiaz subduction

zone, forming the oldest crust in the Melanesian Basin (its present-day remnants residing in the Solomon Sea) (Fig. 14C). Further south, spreading continued in the South Loyalty Basin behind a west-dipping subduction zone (Matthews et al., 2015).

6.2.2. Early Eocene-Late Oligocene

A change in plate boundaries in the SW Pacific between New Caledonia and New Zealand occurred in the Early Eocene at 55 Ma (Cluzel et al., 2006; Crawford et al., 2003; Lagabrielle et al., 2013; Matthews et al., 2015; Ulrich et al., 2010; Whattam et al., 2008), initiating a period of unambiguous subduction east of the Lord Howe Rise (Matthews et al., 2015) (Fig. 14C). This subduction zone initiated the closure of the South Loyalty Basin behind an east-dipping subduction zone possibly along the Loyalty Arc (Matthews et al., 2015), while southwest-dipping subduction was continuing further north along the Vitiaz Trench (Fig. 14C). We connect these two opposite-verging subduction zones via a right-lateral transform boundary along the newly established d'Entrecasteaux Zone (Fig. 14C). This new plate boundary isolated the northern part of the South Loyalty Basin north of the d'Entrecasteaux Zone from the rest of the basin, which was being consumed behind an east-dipping subduction zone along the Loyalty Ridge. As there is no geological or geophysical evidence for subduction north of New Caledonia adjacent to the northern Lord Howe Rise, Kenn Plateau and Mellish Rise, we propose that the trapped piece of the South Loyalty Basin north of the d'Entrecatseaux Zone may underlie the present-day d'Entrecasteaux Basin (zone 1; see Fig. 5 and 8 and 14C). Although we are unable to resolve the age of basin formation from the magnetic anomaly data, this assumption does resolve the difficulty in opening the d'Entrecasteaux Basin based on our understanding of the surrounding plate boundaries, the geometry of the basin itself and the lack of an identifiable extinct ridge. However, fully testing this hypothesis requires age dating of the crust and further magnetic anomaly and

swath bathymetry profiles. The ~55 Ma subduction initiation event may have led to the waning of seafloor spreading in the Tasman and Coral Sea, where spreading ceased by the Early Eocene, at 52 Ma (Gaina et al., 1998; Gaina et al., 1999).

Seafloor-spreading in the Santa Cruz Basin and South Rennell Trough began in the Early Eocene, at ~48 Ma (see section 6.1) (Fig. 13 and 14D). Prior to the opening of this spreading system, we assume that the Rennell Island Ridge and West Torres Plateau formed a continuous ridge, likely volcanic or arc-volcanic in nature. The structural trends observed in the bathymetry and gravity data indicate NW-SE directed motion along the western margin of the West Torres Plateau, consistent with the structural trends (trend T1; Fig. 2) along the Rennell Island Ridge. If this hypothesis is correct, samples from the core of the West Torres Plateau should have similar ages and geochemical affinities to the Rennell Island Ridge. However, as no samples from the West Torres Plateau proper are available, this remains an open question. We model a connection between the NW-SE-directed spreading in the Santa Cruz-South Rennell system with the NE-SW directed spreading in the Melanesian Basin (opening behind the Melanesian Arc) in a triple junction setting, forming a basin that exceeds 2000 km in length (Fig. 14D-E). Triple junctions and spreading centre complexity are common features in back-arc basins (e.g. North Fiji Basin (Auzende et al., 1988), South Fiji Basin (Herzer et al., 2011; Sdrolias et al., 2003), Lau Basin (Taylor et al., 1996), Parece Vela and Shikoku Basins (Sdrolias et al., 2004)). We model the crust forming along the north-western arm of this triple junction (Melanesian Basin component) as being the crust that now underlies the Solomon Sea. The Solomon Sea has been interpreted as opening either from 60-40 Ma (Davies and Price, 1986; Joshima et al., 1986) or 45-30 Ma (Falvey and Pritchard, 1982), with chrons 19-15 (45-35 Ma) identified (Gaina and Müller, 2007). These ages are consistent with the timing of Santa Cruz-South Rennell opening (Fig. 14D-E).

To accommodate the NW-SE-directed opening of the Santa Cruz-South Rennell spreading system, compression or convergence would have occurred either to the northwest or southeast. Indications of subduction activity along the d'Entrecasteaux Zone during the time of basin opening (48-25 Ma) are sparse but arc/BAB type basalts with age ranges of around 30-38 Ma have been reported (Mortimer et al., 2014). We suggest that the pre-existing short-lived right-lateral transform boundary along the d'Entrecasteaux Zone was a pre-existing zone of weakness, which may have allowed for the localization of subduction during the opening of the Santa Cruz-South Rennell spreading system (Fig. 13 and 14D-E). In our model, approximately 300 km of the trapped South Loyalty Basin crust that now underlies the d'Entrecasteaux Basin was consumed during this southward-dipping subduction phase and may also have induced back-arc spreading in the North Loyalty Basin, dated to have initiated at around 44 Ma (Sdrolias et al., 2003). The southward-dipping subduction along the d'Entrecasteaux Zone connected with the east-dipping subduction along the Loyalty Ridge (Meffre et al., 2012), which was consuming crust formed during South Loyalty Basin spreading (Fig. 14D-E). It is important to note that the concept of this period of subduction along the d'Entrecasteaux Zone is model-dependent.

While spreading continued along the Melanesia-South Rennell-Santa Cruz triple junction between 44-25 Ma (Eocene-Oligocene), subduction was ongoing to the west of the region, north of PNG along the Sepik Arc, consuming back-arc basin crust from the Cretaceous Sepik Basin (Zahirovic et al., in review). We extend this northward-dipping subduction zone towards the southeast, consuming the remainder of the Emo Basin crust (Fig. 14E). The closure and obduction of the Sepik and Emo Basin occurred in the Late Oligocene, at ~30-25 Ma (Zahirovic et al., in review; Zahirovic et al., 2014) synchronous with other collisional events in the area.

6.2.3. Late Oligocene-Miocene

A major change in plate boundary configurations occurred at around 25 Ma in the SW Pacific-SE Asia. The Ontong Java Plateau, the world's largest LIP, is believed to have arrived at the Vitiaz Trench (Fig. 14F) at 25 Ma (Holm et al., 2013; Petterson et al., 1999). The arrival is assumed to be marked by a soft collision with no major associated uplift (Petterson et al., 1999) and it has been proposed that it affected Australian plate motion (Knesel et al., 2008). Although other interpretations for the timing of collision exist (e.g., Oligocene based on paleomagnetic constraints (Musgrave, 2013) and Pliocene based on marine geophysical data (Cowley et al., 2004), we adhere to the 25 Ma age as consistent with the geological record from the Melanesian Arc (Petterson et al., 1999). The youngest rocks dredged from the ridge axis along the South Rennell Trough and Santa Cruz Basin have ages of ~28 Ma (Middle Oligocene) (Mortimer et al., 2014). We suggest that complete cessation of activity along the Melanesia-Santa Cruz-South Rennell system may not have occurred until 25 Ma (Late Oligocene), at which point the collision of the Ontong Java Plateau with the Melanesian Arc would have induced a reconfiguration of plate boundaries on the over-riding plate, leading to a termination of magma supply to the ridge. Southward-dipping subduction, albeit at a reduced rate, continued along the Melanesian subduction zone as the plateau was being subducted. To accommodate continued convergence between the Pacific and Australian plates, we support the concept of southward-directed subduction landward of the Melanesian subduction zone along the Trobriand Trough, as previously suggested by Petterson et al. (1999), Hall (2002), Hill and Hall (2003) and Schellart et al. (2006), and related igneous rock emplacement in the Late Oligocene in the New Guinea Mobile Belt (Cloos et al., 2005; Hill and Raza, 1999). This subduction zone was established after the accretion of the Sepik composite terrane to PNG (Zahirovic et al., in review; Zahirovic et al., 2014) and consumed crust that formed during the earliest stage of Melanesian Basin opening

(Fig. 14F). Within the eastern Coral Sea, we model ~200 km of extension occurring in Zone 2 of the d'Entrecasteaux Basin, translating the West Torres Plateau eastward via right-lateral transform motion along the d'Entrecasteaux Zone (Fig. 13 and 14F). The enigmatic 26 Ma (Late Oligocene) basalt sample from a spur of the West Torres Plateau (Fig. 8) may reflect the initial stages of extension in this small basin. To the southeast of the area, it has been proposed that cessation of South Fiji Basin opening occurred at 25 Ma (Sdrolias et al., 2003). Although recent redating of magnetic anomalies with additional geophysical data has placed the cessation of South Fiji Basin opening at 15 Ma (Herzer et al., 2011), this model implies a change in spreading direction at ~25 Ma.

Continued convergence subsequently caused major uplift and compression along the Melanesian Arc. By the late Miocene (~12 Ma), a reversal in the polarity of subduction occurred (Cooper and Taylor, 1985; Petterson et al., 1999) as continued subduction of the Ontong Java Plateau choked the subduction system during hard collision. Subduction was re-initiated along the present-day South Solomon/San Cristobal Trench at 12 Ma, leading to the subduction of crust from the Melanesian-Santa Cruz-South Rennell spreading system beneath the Pacific Plate (Fig. 14G). Subduction along the Papuan Peninsula continued, forming the Maramuni Arc (Holm et al., 2015) and may have coincided with a subduction zone between the Louisiade Arc and Woodlark Island at 15 Ma (Webb et al., 2014) (Fig. 14G). To the north of the area, subduction along the New Britain trench is believed to have begun in the late Miocene (Cooper and Taylor, 1985; Johnson, 1979) and north-dipping subduction in New Ireland at 12 Ma based on subsidence and local volcanism (Stewart and Sandy, 1988), coincident with the subduction polarity reversal along the Melanesian Arc. To the south, paleomagnetic evidence exists for substantial clockwise rotation of the New Hebrides Arc since the late Miocene (Falvey, 1975; Musgrave and Firth, 1999) and for a large anticlockwise rotation of Fiji starting at or prior to 10 Ma and ceasing at 3 Ma (Taylor et al.,

2000). We model the late stage evolution of New Hebrides and Fiji based on these paleomagnetic results but suggest that the initiation of their rotation was at 12 Ma, consistent with the subduction polarity reversal event in Melanesia (Fig. 14G). We model the abandonment of the Maramuni Arc (related to Trobriand subduction) due to the collision of the Torricelli-Finisterre Terranes and South Caroline Arc with New Guinea from ~15 Ma to form the Papuan Mobile Belt, with a diachronous collision younging eastwards.

6.2.4. Late Miocene-present day

To the north of the eastern Coral Sea, the opening of the Woodlark Basin between the remnant Melanesian Basin (Solomon Sea) and the Pocklington Trough (Fig. 1) occurred from around 7 Ma (Late Miocene) (Fig. 14H). The opening of the Woodlark Basin is modelled using the rates of rotation of 2-4°/Myr (Taylor et al., 1999) from 3.6 million years to present but extended to 7 Ma. These rates of seafloor-spreading may have decreased to 1.9°/Myr in the recent past (Wallace et al., 2014). The Solomon Sea (containing a remnant piece of the Melanesia Basin) lies to the north of the Woodlark Basin. As there is no present-day evidence for subduction between the Woodlark Basin and Solomon Sea (Bird, 2003), our model implies that the Solomon Sea underwent minor rotation tied to the opening of the Woodlark Basin. Subduction is accommodated to the north and west of the Solomon Sea, along the New Britain Trench.

The present-day plate boundary configuration in the area is complex, with some plate boundaries still poorly-defined (Bird, 2003) (Fig. 1 and 14I). The eastern Coral Sea sits at the north-eastern corner of the Australian Plate, where the crust of the Santa Cruz Basin is being actively subducted along the South Solomon/San Cristobal Trench and New Hebrides trenches (Fig. 1, 13 and 14I). The south, west and northwest of the region are tectonically quiescent. Further north, seafloor spreading is active in the Woodlark Basin, where incipient

continental rifting is occurring as the rift intersects with the PNG mainland to the west (Taylor et al., 1995), and ridge subduction/slab window formation where the ridge intersects with the South Solomon/San Cristobal Trench to the east (Chadwick et al., 2009; Crook and Taylor, 1994).

7. Conclusions

We have combined a structural interpretation of swath bathymetry data, petrological and microfossil analysis of dredge samples and an interpretation of marine geophysical data from the eastern Coral Sea to propose a new model for the opening of the Santa Cruz Basin and South Rennell Trough and the wider Melanesian arc and back-arc region. We constrain the opening of the Santa Cruz Basin and South Rennell Trough to between ~48-25 Ma based on a combination of magnetic anomaly interpretations, where chrons 20o-13y have been identified, and age-dating of dredge samples. Geochemical analysis of the basalts from the Rennell Island Ridge and South Rennell Trough shows they resemble E-MORB basalts, similar in composition to the recently re-analysed and dated ORSTOM dredges (Mortimer et al., 2014). The cessation of spreading along the South Rennell Trough, Santa Cruz Basin and Melanesia Basin/Solomon Sea occurred by at least 28 Ma with possible complete termination by 25 Ma, corresponding to a regional reorganization of the plate boundaries in the area, possibly attributed to the initial soft collision of the Ontong Java Plateau.

Our model proposes that the Melanesian Basin (Solomon Sea) began at ~61 Ma and by 48 Ma was simultaneously opening with the Santa Cruz-South Rennell spreading system in a triple junction configuration. The 55 Ma major change in plate boundary configurations in the SW Pacific south of New Caledonia led to the establishment of the d'Entrecasteaux Zone as a plate boundary, separating the SW Pacific from the Melanesian-SE Asia region and may have trapped South Loyalty Basin crust in the present-day d'Entrecasteaux

Basin. Complexity in the plate boundaries in the area started from around 48 Ma, with the establishment of the Melanesia-Santa Cruz-South Rennell spreading system, with two subduction zones in the area by 40 Ma, one along the Melanesian/Vitiaz Arc bordering the Pacific Plate and another close to PNG along the Sepik Arc, with the latter likely active since the Late Cretaceous. This initiated a period of subduction zone complexity, whereby crust created in the Melanesian Basin was being actively subducted. The 25 Ma regional plate reorganization event is reflected in the cessation of back-arc basin activity, the establishment of the Maramuni subduction zone along PNG and the isolation of the Solomon Sea Plate. This was followed by a reorganization of plate boundaries at 12 Ma, leading to the establishment of northward-dipping subduction along the South Solomon and New Hebrides subduction zones and setting the scene for the present-day configuration of plate boundaries.

Our plate reconstructions, which include a network of continuously closing plate boundaries can form the basis of a model of plate boundary continuity between the SW Pacific and SE Asia throughout the Cenozoic, and can be used to address questions such as the behaviour of intra-oceanic subduction zones and their relationship to back-arc processes and major oceanic plateau accretion events.

Acknowledgements

We thank the Captain and crew of *R/V Southern Surveyor* and Australia's Marine National Facility (MNF) for the success of voyage *SS2012_V06*. Mineral separation was done by John Simes and Belinda Smith Lyttle. We thank Hugh Davies for his attempts to locate old Solomon Sea dredge samples. We thank Geoscience Australia and New Caledonia agencies for voyage support. We would like to acknowledge funding from the Australian Research Council through grants DP0987713 and FT130101564 (MS), FL0992245 (SEW),

IH130200012 (SZ) and DP130101946 (KJM). Support from the New Zealand Government through core funding to GNS Science (NM) is also acknowledged.

Figures

Figure 1: Regional bathymetry compilation of the eastern Coral Sea from Geoscience Australia, with hill-shade using gravity gradients from Sandwell et al. (2014). Red stars mark the location of dredges from voyage SS2012_V06 used in this study, white stars mark the location of dredges from voyage SS2012_V06 not used in this study and grey line denotes the ship track from voyage *SS2012_V06*. Rennell Island is coloured white as opposed to other land coloured light yellow. BP = Bellona Plateau, CSB = Coral Sea Basin, DEZ = d'Entrecasteaux Zone, ELR = East Lapérouse Rise, LHR = Lord Howe Rise, NCB = New Caledonia Basin, NCR = New Caledonia Ridge, NLB = North Loyalty Basin, RI = Rennell Island, WLR = West Lapérouse Rise, WSB = West Santo Basin.

Figure 2: Regional Geoscience Australia bathymetry compilation with gravity gradients (Sandwell et al., 2014) for the Rennell Island Ridge and Rennell Basin. Plate boundaries are from Bird (2003). The two main structural trends in the region are marked as black dotted lines. Localised structural interpretation from bathymetry and gravity data shown as orange lines, dredge locations from voyage SS2012_V06 marked as red stars, other dredge locations marked as green stars. ELR = East Lapérouse Rise, LP = Louisiade Plateau, LT = Louisiade Trough, SCB = Santa Cruz Basin, SRT = South Rennell Trough, WLR = West Lapérouse Rise.

Figure 3: Basemap and key same as in Fig. 2 but for the South Rennell Trough. BP = Bellona Plateau.

Figure 4: Basemap and key same as in Fig. 2 but for the Santa Cruz Basin. A detailed view of the swath bathymetry data can be found in Fig. S2.

Figure 5: Basemap and key same as in Fig. 2 but for the West Torres Plateau and d'Entrecasteaux Basin. A detailed view of the swath bathymetry data can be found in Fig. S3.

Figure 6: Summary of new rock types with microfossil and Ar-Ar ages from samples dredged on voyage SS2012_V06.

Figure 7: An Al2O3 vs TiO2 bivariate plot with chrome spinel geochemistry from four dredge sites and reference fields from Kamenetsky et al. (2001). Sample DR2H has affinities with arc-related basalts, indicating the sediments around Rennell Island derived from an eroding volcanic source. In contrast, DR4B from the West Torres Plateau is of an N-MORB rather than arc-related origin. Samples DR6 and DR14iii, from the East Lapérouse Rise and the South Rennell Trough, are both transitional to arc-related basalts, consistent with an E-MORB chemistry. Abbreviations of locations in key same as Fig. 2.

Figure 8: Argon-argon degassing spectra for six plagioclase and groundmass separates. Corresponding K/Ca ratios are in green. Uncertainties shown in this figure are ±2σ. TFA=total fusion age, WMPA=statistically valid weighted mean plateau age, PseudoPA=subjectively selected pseudoplateau age.

Figure 9: Binary diagrams illustrating the enriched mid-ocean ridge basalt (E-MORB) nature of lavas from the South Rennell Trough spreading system (green symbols). **A**. Ti vs V after Shervais (1982); **B**. Nb/Yb vs Th/Yb after Pearce (2008). New data shown in symbols with thick black borders. Other data from Davies and Price (1986), Peate et al. (1997) and (Mortimer et al., 2012; Mortimer et al., 2014; Mortimer et al., 2007). N-MORB-normal mid-ocean ridge basalt, BABB=back-arc basin basalt, OIB=ocean island basalt.

Figure 10: Magnetic anomaly profiles over the Santa Cruz Basin. Pink profiles are from existing publicly available datasets, blue profiles are from the ECOSAT survey presented in this paper. Shiptrack profile names used in Figure 11 are annotated. Dredge samples are marked as red stars (this study) and green stars from Mortimer et al. (2014). Dredge samples (this study) with reported Ar-Ar ages are annotated. Plate boundaries are from Bird (2003). Magnetic anomaly identifications are presented as coloured circles (see key for chrons and ages).

Figure 11: Stacked magnetic anomaly profiles for the Santa Cruz Basin. Ship profiles used as annotated and labelled on Figure 10. Synthetic profile was created using the Modmag software (Mendel et al., 2005) assuming a magnetic source layer at a depth of 4 km, with a thickness of 0.5 km, magnetization of 10 A/m, and a contamination coefficient of 0.5. Modelled spreading rates of 45 mm/yr (chrons 20-18) and 30 mm/yr (chrons 18-13) were used for the main period of basin opening, while 10 mm/yr was used to model the waning of the spreading system to the extinct ridge at 25 Ma.

Figure 12: Magnetic anomaly profiles over the d'Entrecasteaux Basin. Pink profiles are from existing publicly available datasets, blue profiles are from voyage SS2012_V06 presented in this paper. Dredge samples are marked as red stars (this study) and green stars from Mortimer et al. (2014). Dredge samples (this study) with reported Ar-Ar ages are annotated. Plate boundaries are from Bird (2003). Magnetic anomaly interpretation of Lapouille (1982) plotted as light blue dotted lines.

Figure 13: Plate tectonic reconstructions in a fixed Australia reference frame for the Santa Cruz Basin/South Rennell Trough region starting at 52 Ma (marks the end of spreading in the Tasman and Coral Seas and Louisiade Trough) to the present-day. Coloured polygons denote different plates involved in the system (see key for plate names). Plate boundaries are

marked in black (refer to Fig. 14 for names of plate boundary features), with open triangles for the subduction zones denoting model-dependent convergence. Main bathymetric features shown as thin black outlines. Green line denotes the South Rennell spreading axis: active (solid), waning (dashed), extinct (dotted). ELR = East Lapérouse Rise, KP = Kenn Plateau, LP = Louisiade Plateau, MR = Mellish Rise, NBP = North Bellona Plateau, RIR = Rennell Island Ridge, WLR = West Lapérouse Rise, WTP = West Torres Plateau.

Figure 14: Regional plate tectonic reconstructions in a mantle frame of reference for the SW Pacific from 85 Ma to the present-day. Plate boundaries are marked in black, with open triangles for subduction zones denoting model-dependent convergence. Basemap shows the age of the oceanic crust in the region. Purple polygons are volcanic related products from the region, including Large Igneous Provinces and hotspot trails (note that the Louisiade Plateau is tentatively marked as a LIP, see Section 2). Main plates are labelled in bold black text: AUS = Australia, CS = Caroline Sea, PAC = Pacific, PMP = Proto-Molucca, PSP = Philippine Sea, SFP = South Fiji, SSP = Solomon Sea. Features mentioned in text are annotated in grey text: CSB = Coral Sea Basin, DEB = d'Entrecasteaux Basin, DEZ = d'Entrecasteaux Zone, EM = Emo Basin, ESZ = Emo subduction zone, LHR = Lord Howe Rise, MA = Melanesia Arc, MB = Melanesia Basin, MSZ = Maramuni subduction zone, NFB = North Fiji Basin, NHA = New Hebrides Arc, NHSZ = New Hebrides subduction zone, NLB = North Loyalty Basin, OJP = Ontong Java Plateau, SCSR = Santa Cruz-South Rennell spreading system, SLB = South Loyalty Basin, SLSZ = South Loyalty subduction zone, SOSZ = South Solomon subduction zone, SSZ = Sepik subduction zone, TSZ = Tonga-Kermadec subduction zone, VSZ = Vitiaz subduction zone, WB = Woodlark Basin.

Table Captions

Table 1. Summary of dredge localities, rock types and analyses.

Table 2. Summary of Ar-Ar dating

References

Acharyya, S.K., 1998. Break-up of the greater Indo-Australian continent and accretion of blocks framing South and East Asia. J. Geodyn. 26, 149-170.

Auzende, J.-M., Lafoy, Y., Marsset, B., 1988. Recent geodynamic evolution of the north Fiji basin (southwest Pacific). Geology 16, 925-929.

Belford, D., 1976. Appendix: Foraminifera and age of samples from south-eastern Papua. Geology of the South-eastern Papuan Mainland, Bull. Bur. Miner. Resour., Geol. Geophys., Aust 165, 73-82.

Bird, P., 2003. An updated digital model of plate boundaries. Geochemistry, Geophysics, Geosystems 4, 1027, doi:1010.1029/2001GC000252.

Boyden, J.A., Müller, R.D., Gurnis, M., Torsvik, T.H., Clark, J.A., Turner, M., Ivey-Law, H., Watson, R.J., Cannon, J.S., 2011. Next-generation plate-tectonic reconstructions using GPlates, In: Keller, G.R., and Baru, C (Ed.), Geoinformatics: Cyberinfrastructure for the Solid Earth Sciences. Cambridge University Press, pp. 95-114.

Bryan, S.E., Ernst, R.E., 2008. Revised definition of large igneous provinces (LIPs). Earth-Science Reviews 86, 175-202.

Buck, W.R., Lavier, L.L., Poliakov, A.N., 2005. Modes of faulting at mid-ocean ridges. Nature 434, 719-723.

Buys, J., Spandler, C., Holm, R.J., Richards, S.W., 2014. Remnants of ancient Australia in Vanuatu: Implications for crustal evolution in island arcs and tectonic development of the southwest Pacific. Geology 42, 939-942.

Chadwick, J., Perfit, M., McInnes, B., Kamenov, G., Plank, T., Jonasson, I., Chadwick, C., 2009. Arc lavas on both sides of a trench: Slab window effects at the Solomon Islands triple junction, SW Pacific. Earth and Planetary Science Letters 279, 293-302.

Chaproniere, G.C., 1984. The Neogene larger foraminiferal sequence in the Australian and New Zealand regions, and its relevance to the East Indies letter stage classification. Palaeogeography, palaeoclimatology, palaeoecology 46, 25-35.

Cloos, M., Sapiie, B., van Ufford, A.Q., Weiland, R.J., Warren, P.Q., McMahon, T.P., 2005. Collisional delamination in New Guinea: The geotectonics of subducting slab breakoff. Geological Society of America Special Papers 400, 1-51.

Cluzel, D., Aitchison, J.C., Picard, C., 2001. Tectonic accretion and underplating of mafic terranes in the Late Eocene intraoceanic fore-arc of New Caledonia (Southwest Pacific): geodynamic implications. Tectonophysics 340, 23-59.

Cluzel, D., Meffre, S., Maurizot, P., Crawford, A.J., 2006. Earliest Eocene (53 Ma) convergence in the Southwest Pacific: evidence from pre‐obduction dikes in the ophiolite of New Caledonia. Terra Nova 18, 395-402.

Cochran, J.R., Kurras, G.J., Edwards, M.H., Coakley, B.J., 2003. The Gakkel Ridge: Bathymetry, gravity anomalies, and crustal accretion at extremely slow spreading rates. Journal of Geophysical Research: Solid Earth (1978–2012) 108.

Coffin, M., Duncan, R., Eldholm, O., Fitton, J., Frey, F., Larsen, H., Mahoney, J., Saunders, A., Schlich, R., Wallace, P., 2006. Large igneous provinces and scientific ocean drilling: Status quo and a look ahead. Oceanography 19, 150-160.

Coleman, P.J., Packham, G.H., 1976. The Melanesian Borderlands and India—Pacific plates' boundary. Earth-Science Reviews 12, 197-233.

Cooper, P.A., Taylor, B., 1985. Polarity reversal in the Solomon Islands arc.
Cowley, S., Mann, P., Coffin, M., Shipley, T.H., 2004. Oligocene to Recent tectonic history of the Central Solomon intra-arc basin as determined from marine seismic reflection data and compilation of onland geology. Tectonophysics 389, 267-307.
Cowley, S., Mann, P., Gahagan, L., 1998. Tectonic history of the northern Louisiade Plateau based on deep penetration seismic reflection lines. Eos Trans. AGU 79, 870.
Crawford, T., Meffre, S., Symonds, P.A., 2003. Tectonic Evolution of the SW Pacific: Lessons for the Geological Evolution of the Tasman Fold Belt System in eastern Australia from 600 to 220 Ma., In: Hillis, R., Müller, R.D. (Eds.), Evolution and Dynamics of the Australian Plate.
Crook, K.A., Taylor, B., 1994. Stucture and Quaternary tectonic history of the Woodlark triple junction region, Solomon Islands. Marine Geophysical Researches 16, 65-89.
Daniel, J., Jouannic, C., Larue, B.M., Recy, J., 1978. Marine geology of eastern Coral Sea. South Pacific Marine Geological Notes 1, 81-94.
Davies, H., Price, R., 1986. Basalts from the Solomon and Bismarck seas. Geo-marine letters 6, 193-202.
De Broin, C., Aubertin, F., Ravenne, C., 1977. Structure and history of the Solomon-New Ireland region, International Symposium on Geodynamics in the Southwest Pacific. Editions Technip. Paris, pp. 37-50.
Delescluse, M., Funck, T., Dehler, S.A., Louden, K.E., Watremez, L., 2015. The oceanic crustal structure at the extinct, slow to ultra‐slow Labrador Sea spreading center. Journal of Geophysical Research: Solid Earth.
Dick, H.J., Lin, J., Schouten, H., 2003. An ultraslow-spreading class of ocean ridge. Nature 426, 405-412.
Exon, N., Hill, P., Lafoy, Y., Heine, C., Bernardel, G., 2006. Kenn Plateau off northeast Australia: a continental fragment in the southwest Pacific jigsaw. Australian Journal of Earth Sciences 53, 541-564.
Falloon, T.J., Meffre, S., Crawford, A.J., Hoernle, K., Hauff, F., Bloomer, S.H., Wright, D.J., 2014. Cretaceous fore-arc basalts from the Tonga arc: Geochemistry and implications for the tectonic history of the SW Pacific. Tectonophysics 630, 21-32.
Falvey, D., 1975. Part 2. Younger Pacific arcs and the eastern marginal seas: Arc reversals, and a tectonic model for the North Fiji Basin. Exploration Geophysics 6, 47-49.
Falvey, D., Pritchard, T., 1982. Paleomagnetic Evidence for Large Microplate Rotations in the Southwest Pacific: ABSTRACT. AAPG Bulletin 66, 966-966.
Falvey, D.A., Taylor, L.W., 1974. Queensland Plateau and Coral Sea Basin: structural and time-stratigraphic patterns. Exploration Geophysics 5, 123-126.
Gaina, C., Müller, D.R., Royer, J.Y., Stock, J., Hardebeck, J., Symonds, P., 1998. The tectonic history of the Tasman Sea: a puzzle with 13 pieces. Journal of Geophysical Research 103, 12413-12433.
Gaina, C., Müller, R.D., 2007. Cenozoic tectonic and depth/age evolution of the Indonesian gateway and associated back-arc basins. Earth-Science Reviews 83, 177-203.
Gaina, C., Müller, R.D., Royer, J.-Y., Symonds, P., 1999. The tectonic evolution of the Louisiade Triple Junction. Journal of Geophysical Research 104, 12973-12939.
Gee, J., Kent, D., 2007. Source of Oceanic magnetic anomalies and the geomagnetic polarity timescale. Treatrise Geophys 5, 455ñ507.
Golonka, J., 2004. Plate tectonic evolution of the southern margin of Eurasia in the Mesozoic and Cenozoic. Tectonophysics 381, 235-273.

Gurnis, M., Turner, M., Zahirovic, S., DiCaprio, L., Spasojevic, S., Müller, R.D., Boyden, J., Seton, M., Manea, V.C., Bower, D.J., 2012. Plate tectonic reconstructions with continuously closing plates. Computers & Geosciences 38, 35-42.
Hall, R., 2002. Cenozoic geological and plate tectonic evolution of Southeast Asia and the SW Pacific: computer-based reconstructions, models and animations. Journal of Asian Earth Sciences 20, 353-431.
Herzer, R., Barker, D., Roest, W., Mortimer, N., 2011. Oligocene–Miocene spreading history of the northern South Fiji Basin and implications for the evolution of the New Zealand plate boundary. Geochemistry, Geophysics, Geosystems 12.
Hill, K.C., Hall, R., 2003. Mesozoic-Cenozoic evolution of Australia's New Guinea margin in a west Pacific context. Geological Society of America Special Papers 372, 265-290.
Hill, K.C., Raza, A., 1999. Arc–continent collision in Papua Guinea: Constraints from fission track thermochronology. Tectonics 18, 950-966.
Hoffmann, K., Exon, N., Quilty, P., Findlay, C., 2008. Mellish Rise and adjacent deep water plateaus off northeast Australia: new evidence for continental basement from Cenozoic micropalaeontology and sedimentary geology, PESA Eastern Australian Basins Symposium III, pp. 317-323.
Holm, R.J., Spandler, C., Richards, S.W., 2013. Melanesian arc far-field response to collision of the Ontong Java Plateau: geochronology and petrogenesis of the Simuku Igneous Complex, New Britain, Papua New Guinea. Tectonophysics 603, 189-212.
Holm, R.J., Spandler, C., Richards, S.W., 2015. Continental collision, orogenesis and arc magmatism of the Miocene Maramuni arc, Papua New Guinea. Gondwana Research 28, 1117-1136.
Hughes, G.W., Turner, C.C., 1977. Upraised Pacific Ocean floor, southern Malaita, Solomon Islands. Geological Society of America Bulletin 88, 412-424.
Johnson, R., 1979. Geotectonics and volcanism in Papua New Guinea: a review of the late Cainozoic. BMR J. Aust. Geol. Geophys 4, 181-207.
Joshima, M., Okuda, Y., Murakami, F., Kishimoto, K., Honza, E., 1986. Age of the Solomon Sea Basin from magnetic lineations. Geo-Marine Letters 6, 229-234.
Knesel, K.M., Cohen, B.E., Vasconcelos, P.M., Thiede, D.S., 2008. Rapid change in drift of the Australian plate records collision with Ontong Java plateau. Nature 454, 754-757.
Kroenke, L., 1984. Solomon Islands: San Cristobal to Bougainville and Buka, In: Kroenke, L. (Ed.), Cenozoic tectonic development of the southwest Pacific. U.N. ESCAP, pp. 47-61.
Lagabrielle, Y., Chauvet, A., Ulrich, M., Guillot, S., 2013. Passive obduction and gravity-driven emplacement of large ophiolitic sheets: The New Caledonia ophiolite (SW Pacific) as a case study? Bulletin de la Société Géologique de France 184, 545-556.
Landmesser, C., Andrews, J., Packham, G., 1973. Aspects of the geology of the eastern Coral Sea and the western New Hebrides Basin. Initial Reports of the Deep Sea Drilling Project 30, 647-662.
Lapouille, A., 1982. …TUDE DE~ BASSINSMARGINAUXFOSSILES DUSUD-OUESTPACIFIQUE: BASSINNORD-D'ENTRECASTEAUX, BASSIN NORD-LOYAUT…, BASSIN SUD-FIDJIEN.
Larue, B., Daniel, J., Jouannic, C., Recy, J., 1977. The South Rennell Trough: Evidence for a fossil spreading zone, p. 51ñ61.
Leng, W., Gurnis, M., 2015. Subduction initiation at relic arcs. Geophysical Research Letters 42, 7014-7021.
Lindley, D., 1988. Early Cainozoic stratigraphy and structure of the Gazelle Peninsula, east New Britain: An example of extensional tectonics in the New Britain arc-trench complex. Journal of the Geological Society of Australia 35, 231-244.

Lus, W.Y., McDougall, I., Davies, H.L., 2004. Age of the metamorphic sole of the Papuan Ultramafic Belt ophiolite, Papua New Guinea. Tectonophysics 392, 85-101.
Luyendyk, B.P., Bryan, W., Jezek, P., 1974. Shallow structure of the New Hebrides island arc. Geological Society of America Bulletin 85, 1287-1300.
Maillet, P., Monzier, M., Selo, M., Storzer, D., 1983. The d'Entrecasteaux zone (southwest Pacific). A petrological and geochronological reappraisal. Marine Geology 53, 179-197.
Matthews, K.J., Williams, S.E., Whittaker, J.M., Müller, R.D., Seton, M., Clarke, G.L., 2015. Geologic and kinematic constraints on Late Cretaceous to mid Eocene plate boundaries in the southwest Pacific. Earth-Science Reviews 140, 72-107.
Meffre, S., Falloon, T.J., Crawford, T.J., Hoernle, K., Hauff, F., Duncan, R.A., Bloomer, S.H., Wright, D.J., 2012. Basalts erupted along the Tongan fore arc during subduction initiation: Evidence from geochronology of dredged rocks from the Tonga fore arc and trench. Geochemistry, Geophysics, Geosystems 13.
Mendel, V., Munschy, M., Sauter, D., 2005. MODMAG, a MATLAB program to model marine magnetic anomalies. Computers & geosciences 31, 589-597.
Metcalfe, I., 2009. Late Palaeozoic and Mesozoic tectonic and palaeogeographical evolution of SE Asia. Geological Society, London, Special Publications 315, 7-23.
Michael, P., Langmuir, C., Dick, H., Snow, J., Goldstein, S., Graham, D., Lehnert, K., Kurras, G., Mühe, R., Edmonds, H., 2003. Magmatic and amagmatic seafloor spreading at the slowest mid-ocean ridge: Gakkel Ridge. Arctic Ocean, Nature 423, 956-961.
Morimer, N., Gans, P., Meffre, S., Martin, C., Seton, M., Williams, S., Turnbull, R., Quilty, P., Micklethwaite, S., Sutherland, R., Bache, F., Timm, C., Collot, J., Maurizot, P., Rollet, N., in review. Regional volcanism of northern Zealandia: post-Gondwana breakup magmatism on an extended, submerged continent, In: Sensarma, S., Storey, B. (Eds.), Geological Society of London Special Publications.
Mortimer, N., Gans, P., Hauff, F., Barker, D., 2012. Paleocene MORB and OIB from the Resolution Ridge, Tasman Sea. Australian Journal of Earth Sciences 59, 953-964.
Mortimer, N., Gans, P.B., Palin, J.M., Herzer, R.H., Pelletier, B., Monzier, M., 2014. Eocene and Oligocene basins and ridges of the Coral Sea‐New Caledonia region: Tectonic link between Melanesia, Fiji, and Zealandia. Tectonics 33, 1386-1407.
Mortimer, N., Herzer, R., Gans, P., Laporte-Magoni, C., Calvert, A., Bosch, D., 2007. Oligocene–Miocene tectonic evolution of the South Fiji Basin and Northland Plateau, SW Pacific Ocean: evidence from petrology and dating of dredged rocks. Marine Geology 237, 1-24.
Mühe, R., Bohrmann, H., Garbe-Schönberg, D., Kassens, H., 1997. E-MORB glasses from the Gakkel Ridge (Arctic Ocean) at 87 N: evidence for the Earth's most northerly volcanic activity. Earth and Planetary Science Letters 152, 1-9.
Müller, R., Seton, M., Zahirovic, S., Williams, S., Matthews, K., Wright, N., Shephard, G., Maloney, K., Barnett-Moore, N., Hosseinpour, M., Bower, D., Cannon, J., 2016. Ocean basin evolution and global-scale plate reorganization events since Pangea breakup. Annual Review of Earth and Planetary Sciences 44.
Musgrave, R.J., 2013. Evidence for Late Eocene emplacement of the Malaita Terrane, Solomon Islands: Implications for an even larger Ontong Java Nui oceanic plateau. Journal of Geophysical Research: Solid Earth 118, 2670-2686.
Musgrave, R.J., Firth, J.V., 1999. Magnitude and timing of New Hebrides Arc rotation: paleomagnetic evidence from Nendo, Solomon Islands. Journal of Geophysical Research: Solid Earth (1978–2012) 104, 2841-2853.
Nauret, F., Snow, J., Hellebrand, E., Weis, D., 2011. Geochemical composition of K-rich lavas from the Lena Trough (Arctic Ocean). Journal of Petrology, egr024.

Pearce, J.A., 2008. Geochemical fingerprinting of oceanic basalts with applications to ophiolite classification and the search for Archean oceanic crust. Lithos 100, 14-48.
Peate, D.W., Pearce, J.A., Hawkesworth, C.J., Colley, H., Edwards, C.M., Hirose, K., 1997. Geochemical variations in Vanuatu arc lavas: the role of subducted material and a variable mantle wedge composition. Journal of Petrology 38, 1331-1358.
Petterson, M., Babbs, T., Neal, C., Mahoney, J., Saunders, A., Duncan, R., Tolia, D., Magu, R., Qopoto, C., Mahoa, H., 1999. Geological–tectonic framework of Solomon Islands, SW Pacific: crustal accretion and growth within an intra-oceanic setting. Tectonophysics 301, 35-60.
Récy, J., Dubois, J., Daniel, J., Dupont, J., Launay, J., 1977. Fossil subduction zones: examples in the South West Pacific.
Sandwell, D.T., Müller, R.D., Smith, W.H., Garcia, E., Francis, R., 2014. New global marine gravity model from CryoSat-2 and Jason-1 reveals buried tectonic structure. science 346, 65-67.
Schellart, W., Lister, G., Toy, V., 2006. A Late Cretaceous and Cenozoic reconstruction of the Southwest Pacific region: tectonics controlled by subduction and slab rollback processes. Earth-Science Reviews 76, 191-233.
Sdrolias, M., R.D., M., Gaina, C., 2003. Tectonic Evolution of the SW Pacific Using Constraints from Back-arc Basins, In: R.R., H., R.D., M. (Eds.), Evolution and Dynamics of the Australian Plate. Geological Society of Australia Special Publication 22 and Geological Society of America Special Paper.
Sdrolias, M., Roest, W.R., M√¨ller, R.D., 2004. An expression of Philippine Sea plate rotation: the Parece Vela and Shikoku basins. Tectonophysics 394, 69-86.
Seton, M., Whittaker, J.M., Wessel, P., Müller, R.D., DeMets, C., Merkouriev, S., Cande, S., Gaina, C., Eagles, G., Granot, R., 2014. Community infrastructure and repository for marine magnetic identifications. Geochemistry, Geophysics, Geosystems 15, 1629-1641.
Shervais, J.W., 1982. Ti-V plots and the petrogenesis of modern and ophiolitic lavas. Earth and planetary science letters 59, 101-118.
Smith, I.E., 2013. The chemical characterization and tectonic significance of ophiolite terrains in southeastern Papua New Guinea. Tectonics 32, 159-170.
Smith, I.E., Davies, H., 1976. Geology of the southeast Papuan mainland. Australian Government Pub. Service.
Stampfli, G.M., Borel, G.D., 2002. A plate tectonic model for the Paleozoic and Mesozoic constrained by dynamic plate boundaries and restored synthetic oceanic isochrons. Earth and Planetary Science Letters 196, 17-33.
Stewart, W., Sandy, M., 1988. Geology of New Ireland and Djaul Islands, northeastern Papua New Guinea.
Tapster, S., Roberts, N., Petterson, M., Saunders, A., Naden, J., 2014. From continent to intra-oceanic arc: Zircon xenocrysts record the crustal evolution of the Solomon island arc. Geology 42, 1087-1090.
Taylor, B., Goodliffe, A., Martinez, F., Hey, R., 1995. Continental rifting and initial sea-floor spreading in the Woodlark basin. Nature 374, 534-537.
Taylor, B., Goodliffe, A.M., Martinez, F., 1999. How continents break up: insights from Papua New Guinea. Journal of Geophysical Research: Solid Earth (1978–2012) 104, 7497-7512.
Taylor, B., Zellmer, K., Martinez, F., Goodliffe, A., 1996. Sea-floor spreading in the Lau back-arc basin. Earth and Planetary Science Letters 144, 35-40.

Taylor, G.K., Gascoyne, J., Colley, H., 2000. Rapid rotation of Fiji: paleomagnetic evidence and tectonic implications. Journal of Geophysical Research: Solid Earth (1978–2012) 105, 5771-5781.
Taylor, G.R., 1973. Preliminary observations on the structural history of Rennell Island, south Solomon Sea. Geological Society of America Bulletin 84, 2795-2806.
Taylor, L., Falvey, D., 1977. Queensland Plateau and Coral Sea Basin: stratigraphy, structure and tectonics. The APEA Journal 17, 13-29.
Tejada, M., Mahoney, J., Duncan, R., Hawkins, M., 1996. Age and geochemistry of basement and alkalic rocks of Malaita and Santa Isabel, Solomon Islands, southern margin of Ontong Java Plateau. Journal of Petrology 37, 361-394.
Todd, E., Gill, J.B., Pearce, J.A., 2012. A variably enriched mantle wedge and contrasting melt types during arc stages following subduction initiation in Fiji and Tonga, southwest Pacific. Earth and Planetary Science Letters 335, 180-194.
Tregoning, P., Tan, F., Gilliland, J., McQueen, H., Lambeck, K., 1998. Present-day crustal motion in the Solomon Islands from GPS observations. Geophysical Research Letters 25, 3627-3630.
Ulrich, M., Picard, C., Guillot, S., Chauvel, C., Cluzel, D., Meffre, S., 2010. Multiple melting stages and refertilization as indicators for ridge to subduction formation: The New Caledonia ophiolite. Lithos 115, 223-236.
Wallace, L.M., Ellis, S., Little, T., Tregoning, P., Palmer, N., Rosa, R., Stanaway, R., Oa, J., Nidkombu, E., Kwazi, J., 2014. Continental breakup and UHP rock exhumation in action: GPS results from the Woodlark Rift, Papua New Guinea. Geochemistry, Geophysics, Geosystems 15, 4267-4290.
Webb, L.E., Baldwin, S.L., Fitzgerald, P.G., 2014. The Early‐Middle Miocene subduction complex of the Louisiade Archipelago, southern margin of the Woodlark Rift. Geochemistry, Geophysics, Geosystems 15, 4024-4046.
Weissel, J.K., Watts, A.B., 1979. Tectonic evolution of the Coral Sea Basin. Journal of Geophysical Research 84, 4572-4582.
Wells, R.E., 1989. Origin of the oceanic basalt basement of the Solomon Islands arc and its relationship to the Ontong Java Plateau--insights from Cenozoic plate motion models. Tectonophysics 165, 219-235.
Whattam, S.A., Malpas, J., Ali, J.R., Smith, I.E., 2008. New SW Pacific tectonic model: Cyclical intraoceanic magmatic arc construction and near‐coeval emplacement along the Australia‐Pacific margin in the Cenozoic. Geochemistry, Geophysics, Geosystems 9.
Willcox, J., Symonds, P., Hinz, K., Bennett, D., 1980. Lord Howe Rise, Tasman Sea-Preliminary geophysical results and petroleum prospects. BMR J. Aust. Geol. and Geophys. 5, 225-236.
Williams, S., Gans, P., Mortimer, N., Meffre, S., Seton, M., 2014. Age-progressive volcanism in the Tasman and Coral seas, AGU Fall Meeting Abstracts, p. 4692.
Worthing, M., Crawford, A., 1996. The igneous geochemistry and tectonic setting of metabasites from the Emo Metamorphics, Papua New Guinea; a record of the evolution and destruction of a backarc basin. Mineralogy and Petrology 58, 79-100.
Yan, C.Y., Kroenke, L.W., 1993. A plate tectonic reconstruction of the Southwest Pacific, 0 100 Ma, In: Berger, W.H., Kroenke, L.W., Mayer, L.A. (Eds.), Proceedings of the Ocean Drilling Program, Scientific Results, College Station, TX, p. 697.
Zahirovic, S., Matthews, K.J., Flament, N., Muller, R., KC, H., Seton, M., Gurnis, M., in review. Tectonic evolution and deep mantle structure of eastern Tethyan domain since the latest Jurassic. Earth Science Reviews.

Zahirovic, S., Seton, M., Müller, R., 2014. The Cretaceous and Cenozoic tectonic evolution of Southeast Asia. Solid Earth 5, 227-273.

Figure 1

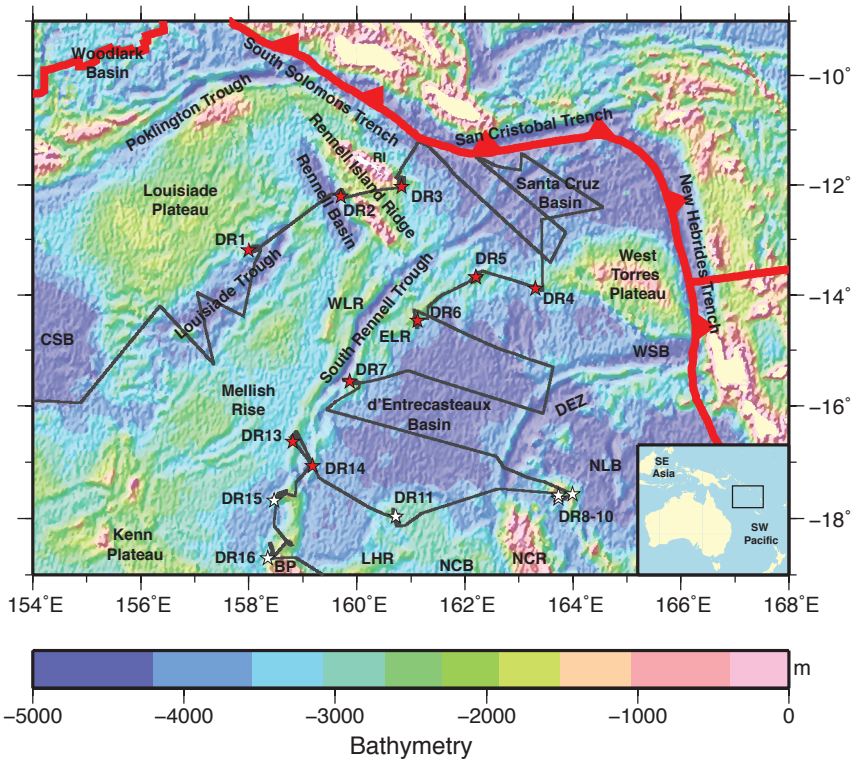

Seton et al. Figure 1

Figure 2

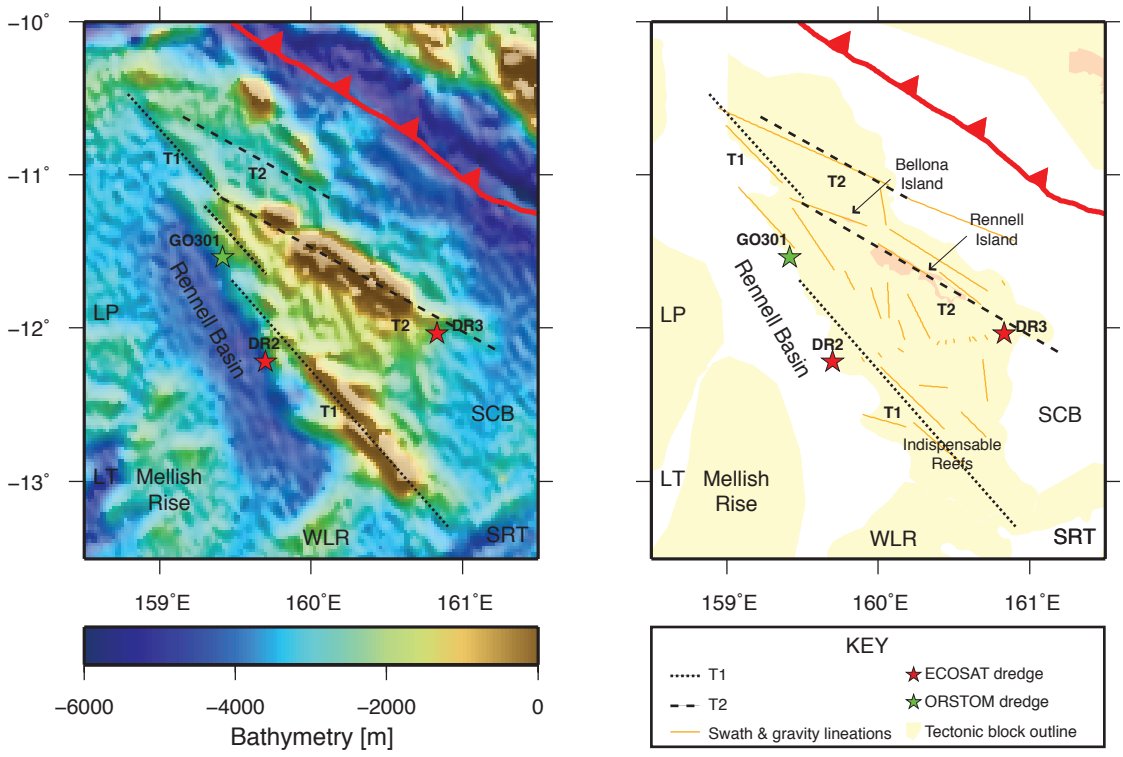
−10˚
−11˚
−12˚
−13˚
159˚E
160˚E
161˚E
T1
T2
GO301
DR2
DR3
Rennell Basin
LP
SCB
LT
Mellish Rise
WLR
SRT
−6000
−4000
−2000
0
Bathymetry [m]
Bellona Island
Rennell Island
Indispensable Reefs
KEY
T1
T2
Swath & gravity lineations
ECOSAT dredge
ORSTOM dredge
Tectonic block outline

Figure 3

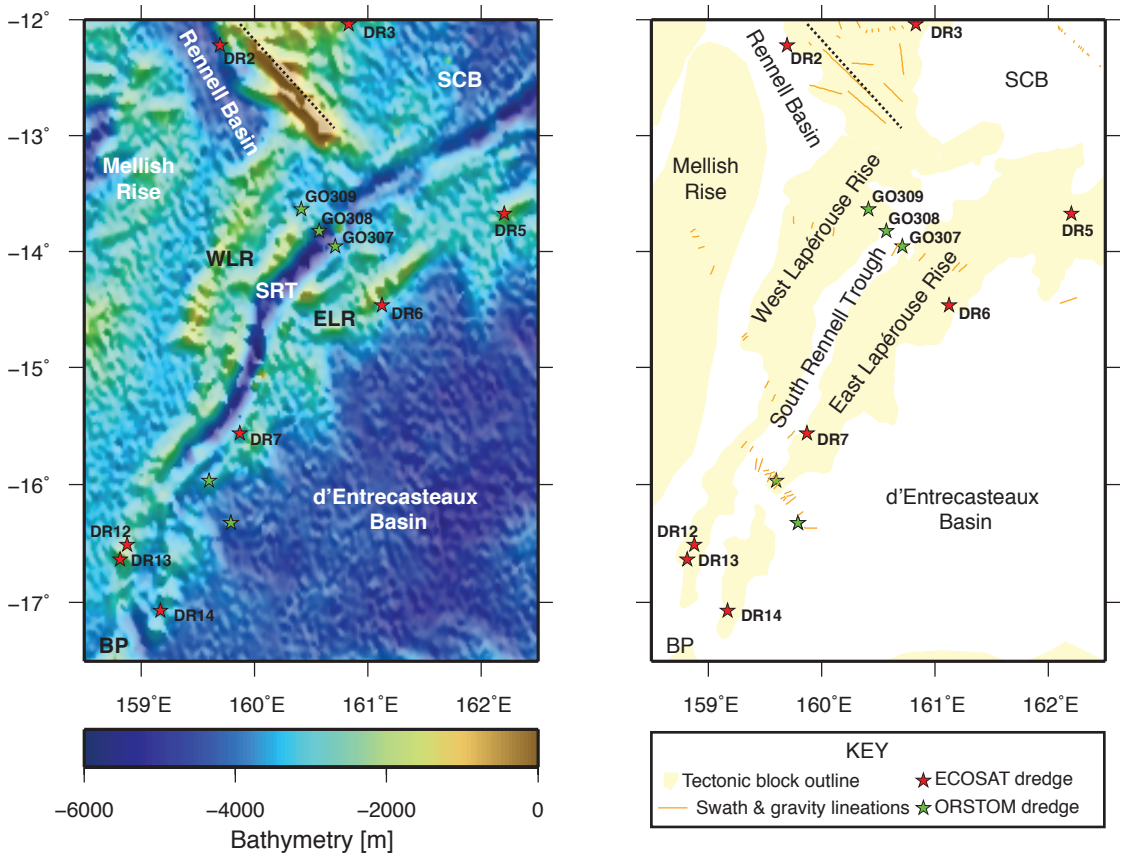
−12˚
−13˚
−14˚
−15˚
−16˚
−17˚
159˚E
160˚E
161˚E
162˚E
DR3
DR2
Rennell Basin
SCB
Mellish Rise
GO309
GO308
GO307
DR5
WLR
SRT
ELR
DR6
DR7
d'Entrecasteaux Basin
DR12
DR13
DR14
BP
−6000
−4000
−2000
0
Bathymetry [m]
West Lapérouse Rise
South Rennell Trough
East Lapérouse Rise
KEY
Tectonic block outline
Swath & gravity lineations
ECOSAT dredge
ORSTOM dredge

Figure 4

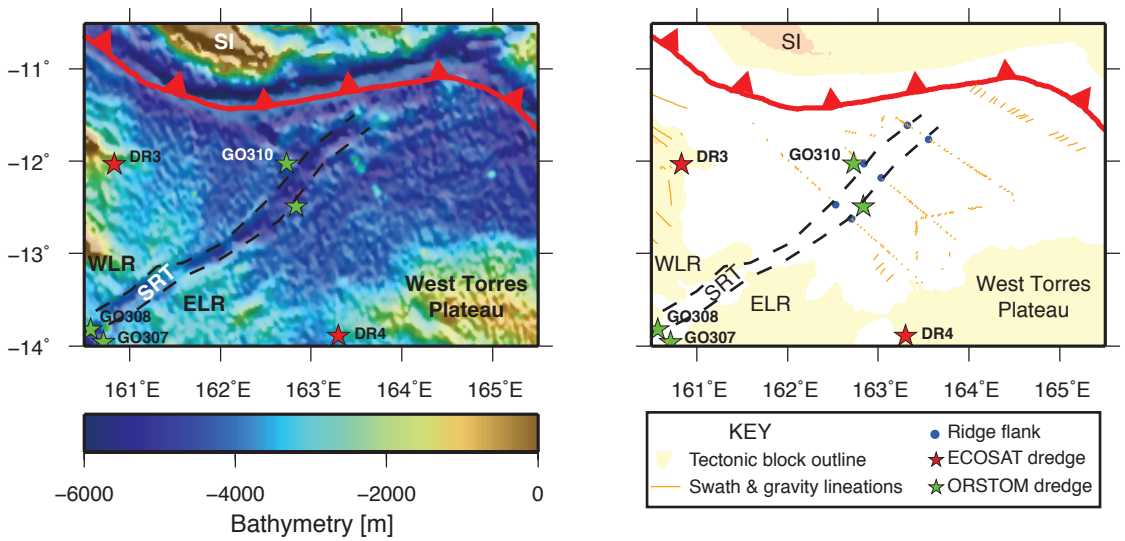
SI
DR3
GO310
WLR
SRT
ELR
West Torres Plateau
GO308
GO307
DR4
−11˚
−12˚
−13˚
−14˚
161˚E
162˚E
163˚E
164˚E
165˚E
−6000
−4000
−2000
0
Bathymetry [m]
KEY
Tectonic block outline
Swath & gravity lineations
Ridge flank
ECOSAT dredge
ORSTOM dredge

Figure 5

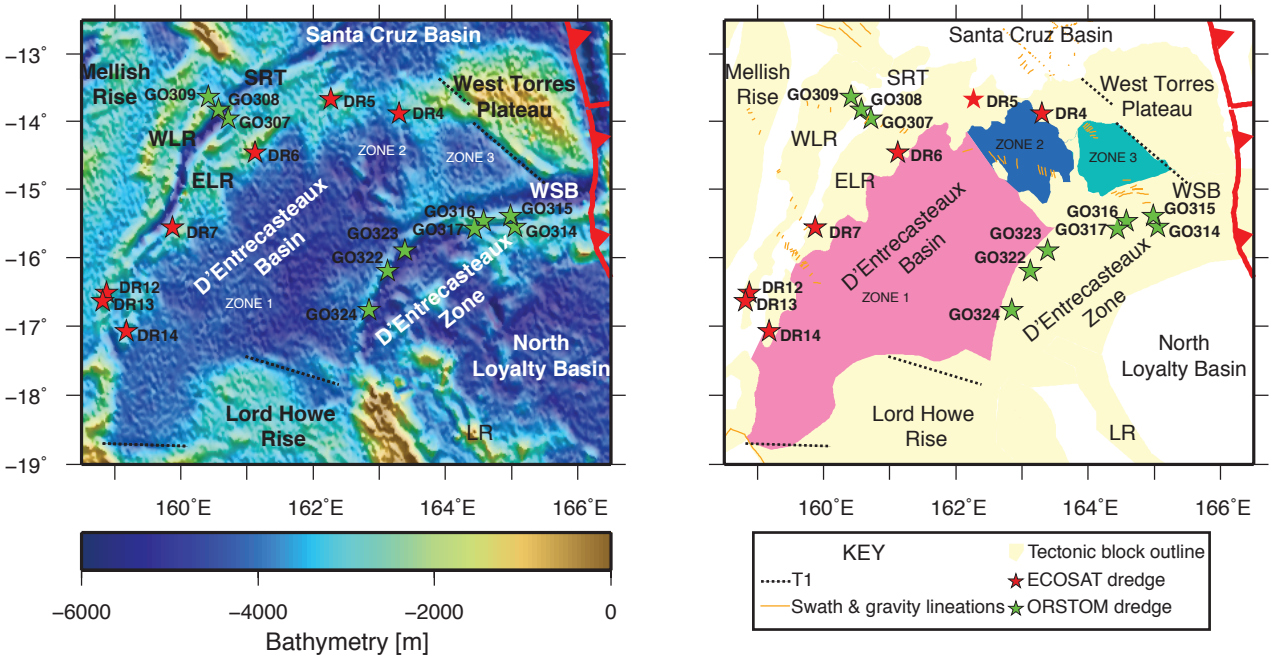

Seton et al. Fig. 5

Figure6

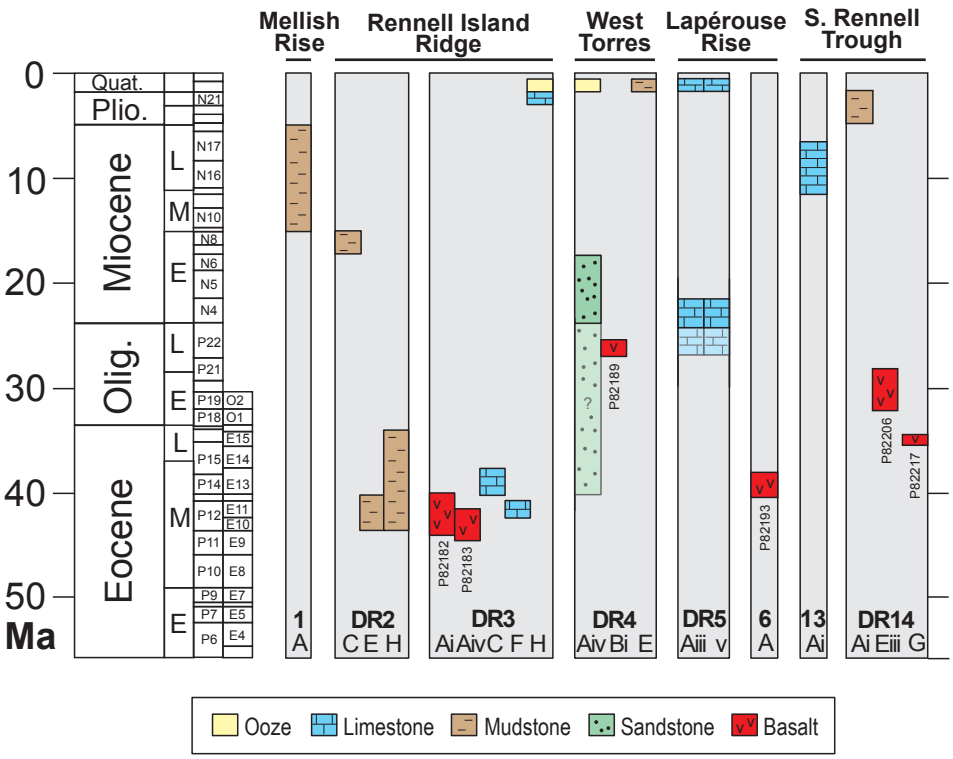

Fig. 6 Seton et al.

Figure 7

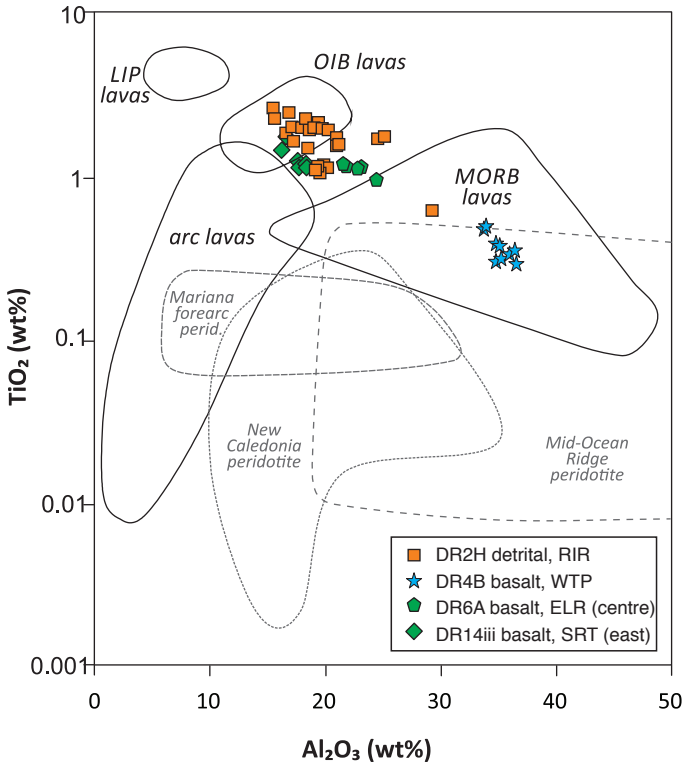

Fig. 7. Seton et al.

Figure8

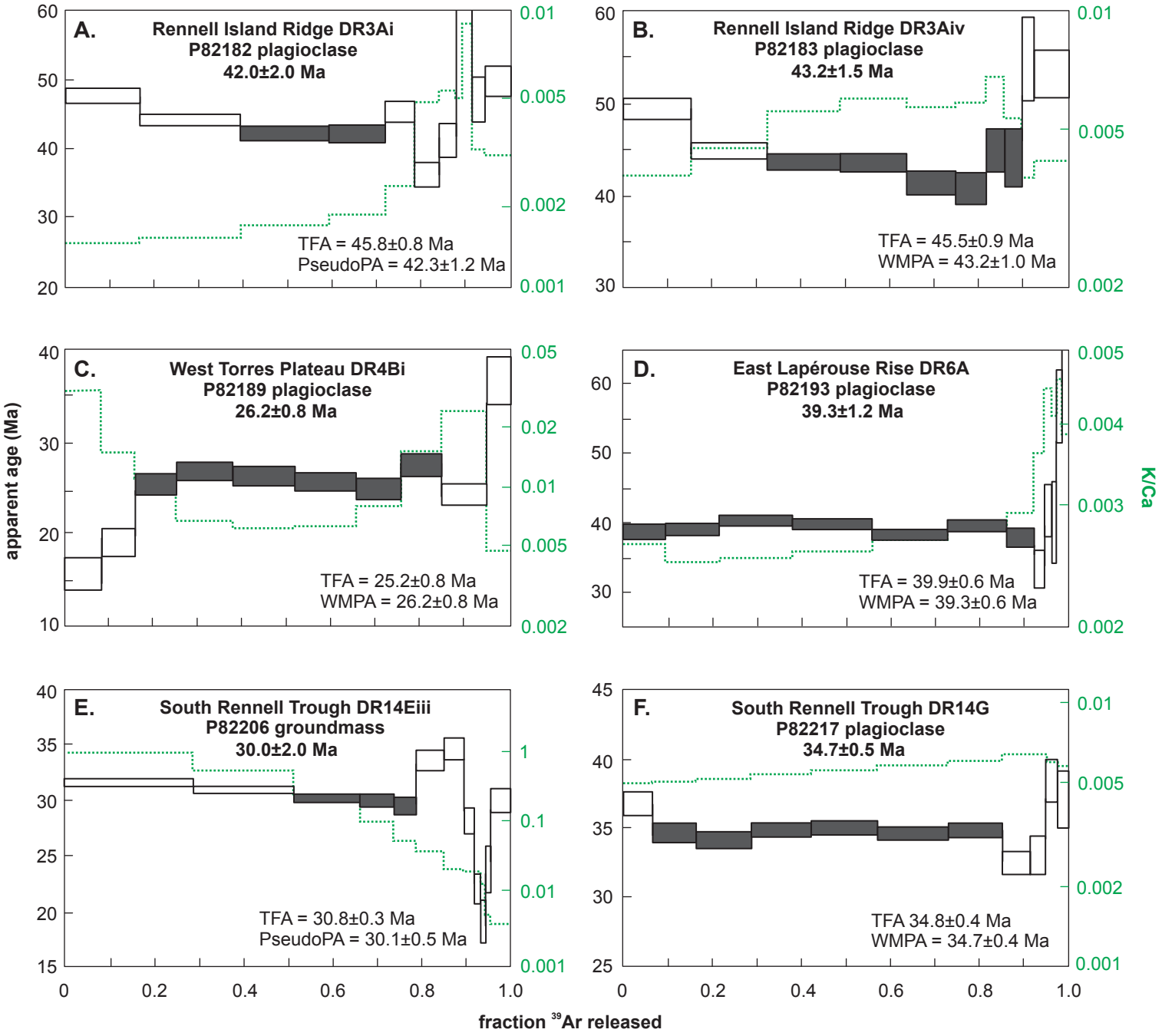

Fig. 8. Seton et al.

Figure9

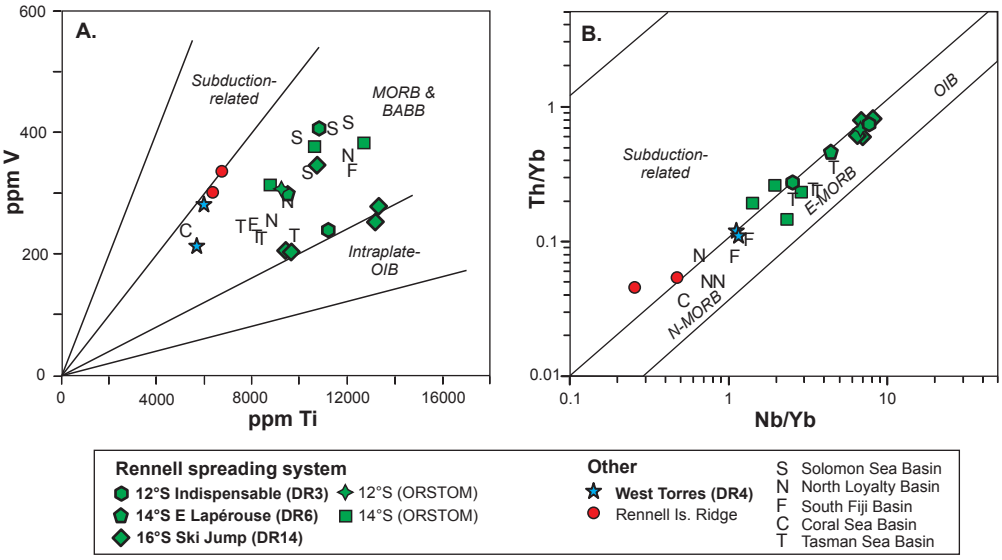

Fig. 9. Seton et al.

Figure 10

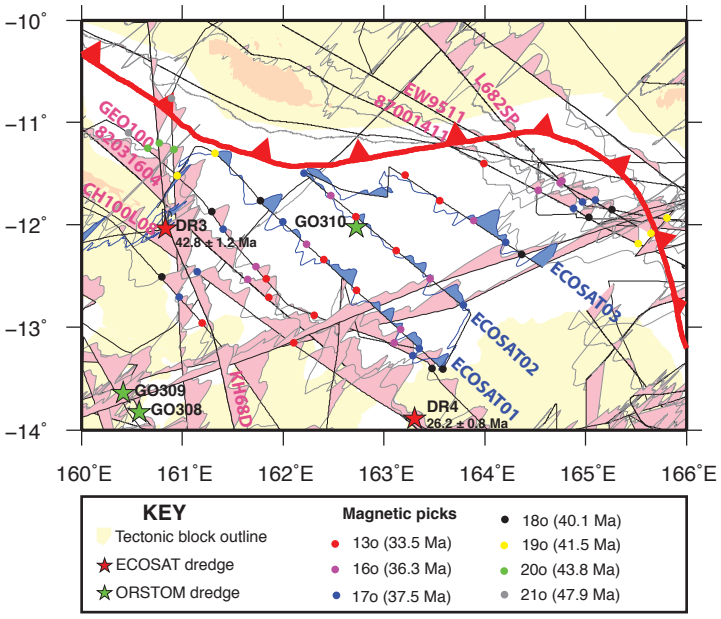

Seton et al. Fig. 10

Figure11

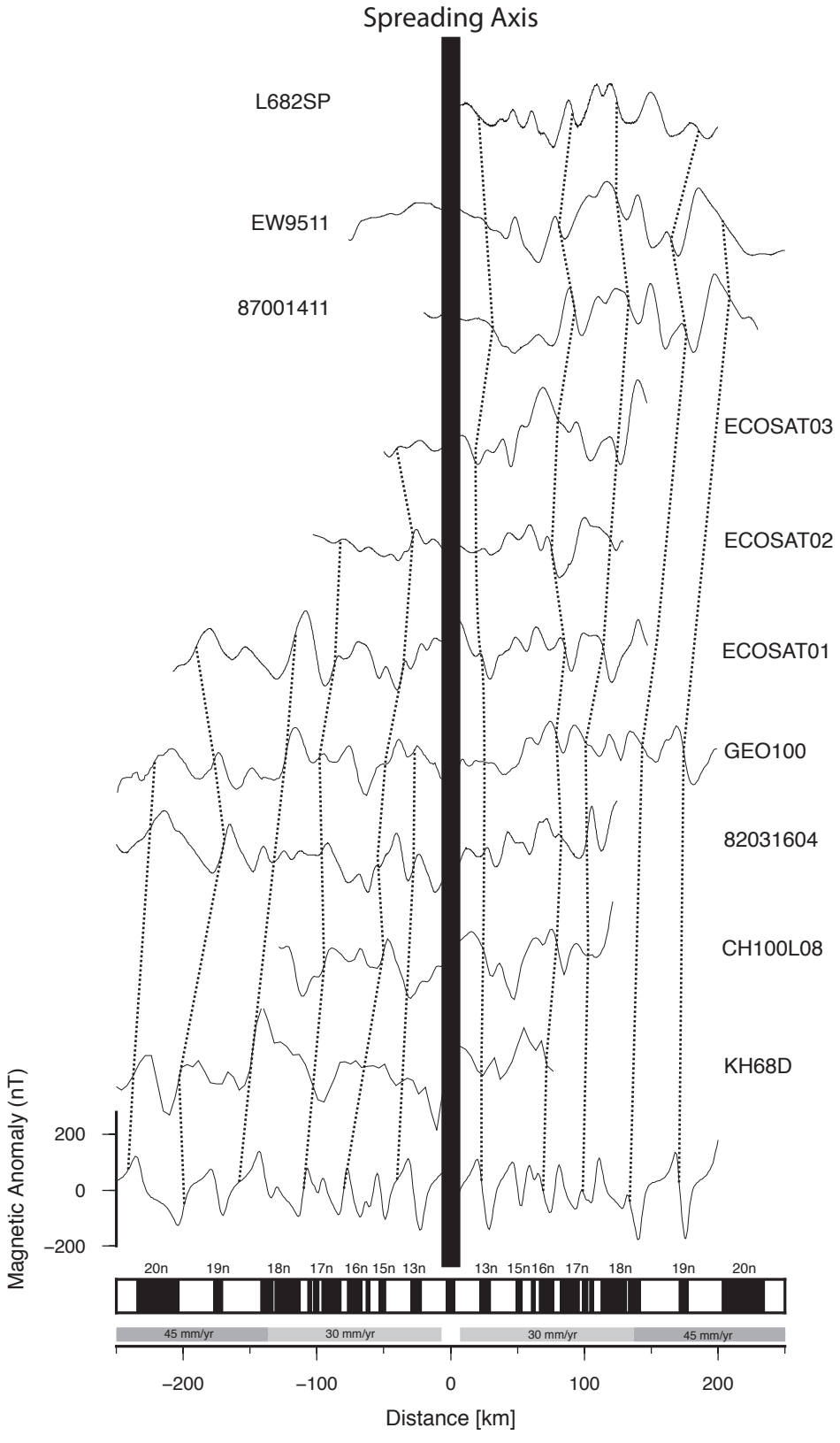

Seton et al. Fig. 11

Figure 12

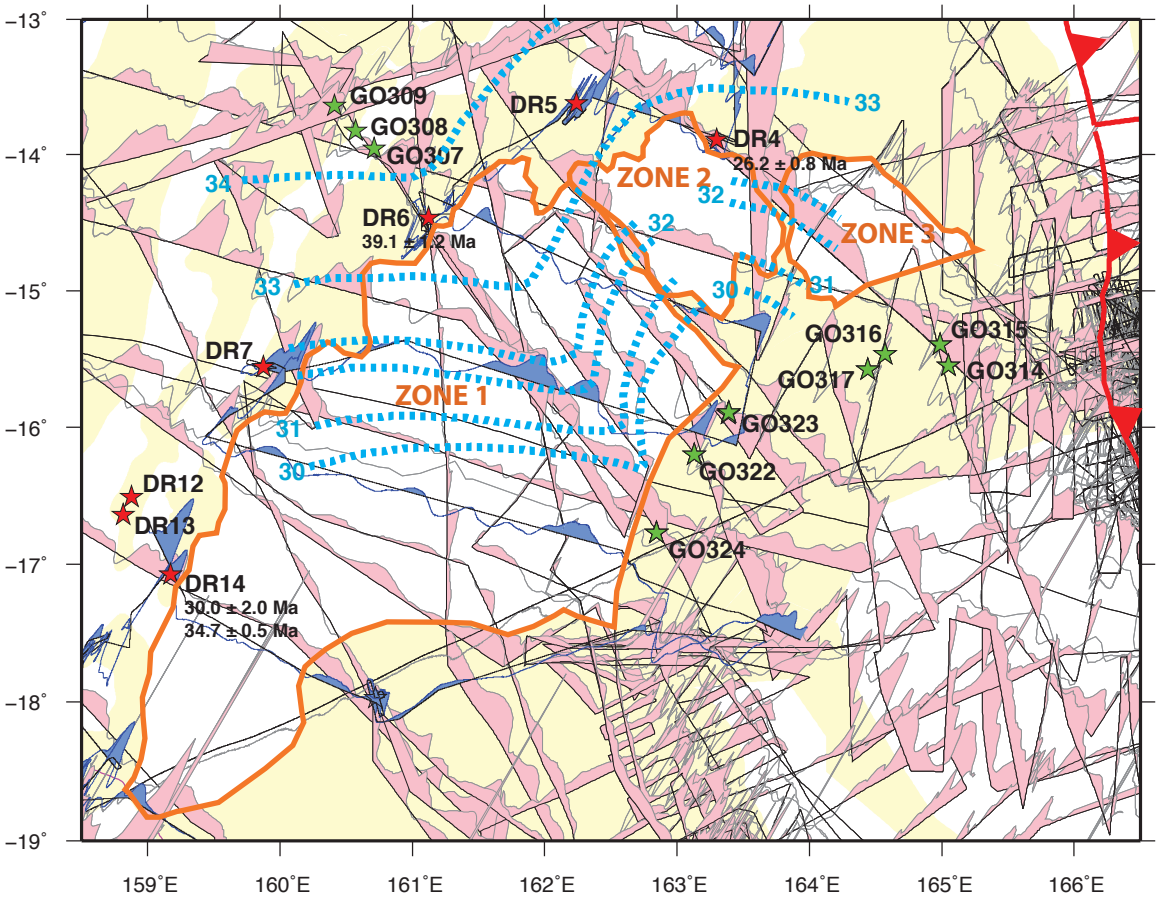

Seton et al. Fig. 12

Figure 13

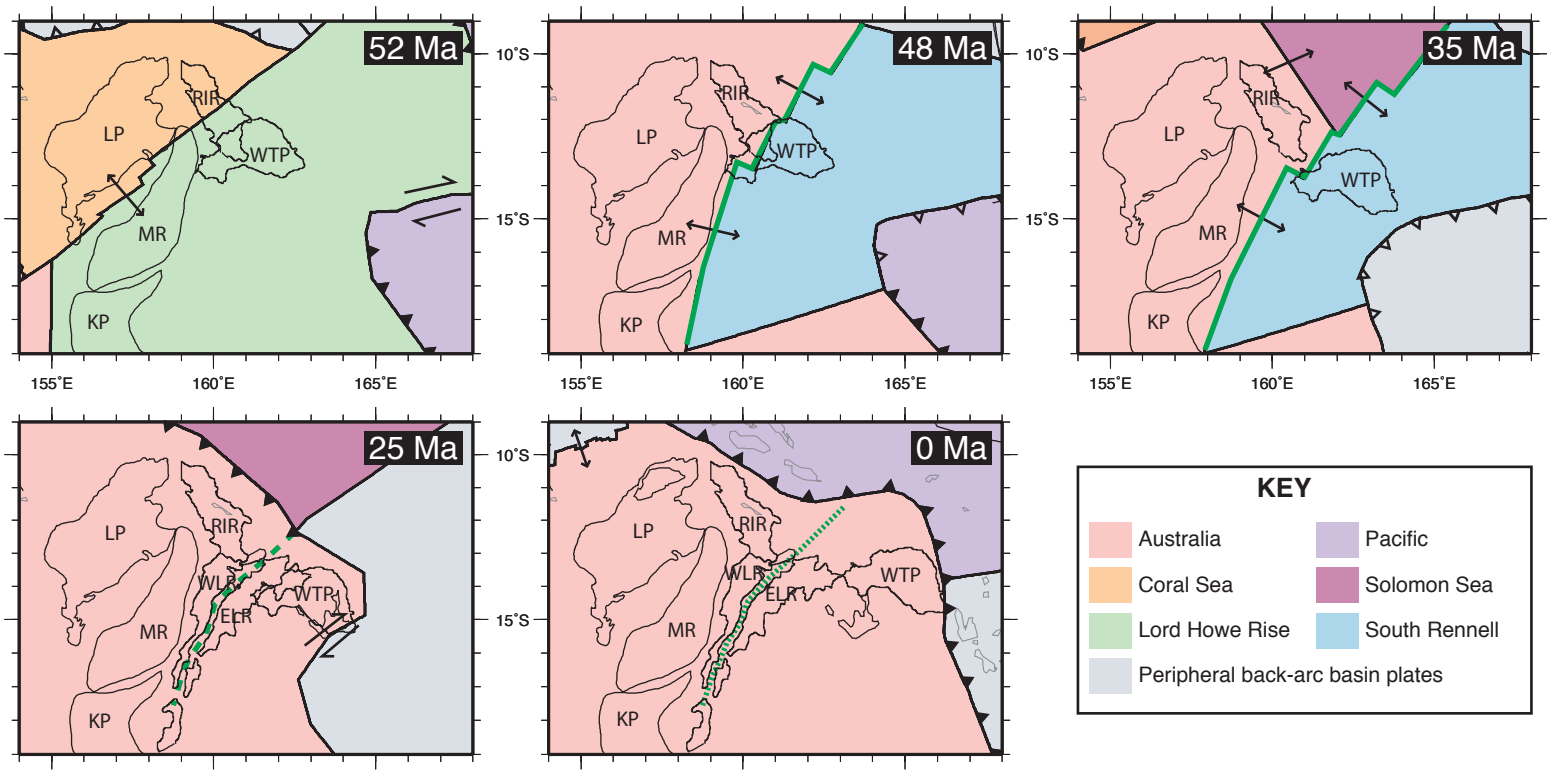

Fig. 13 Seton et. al.

Figure 14

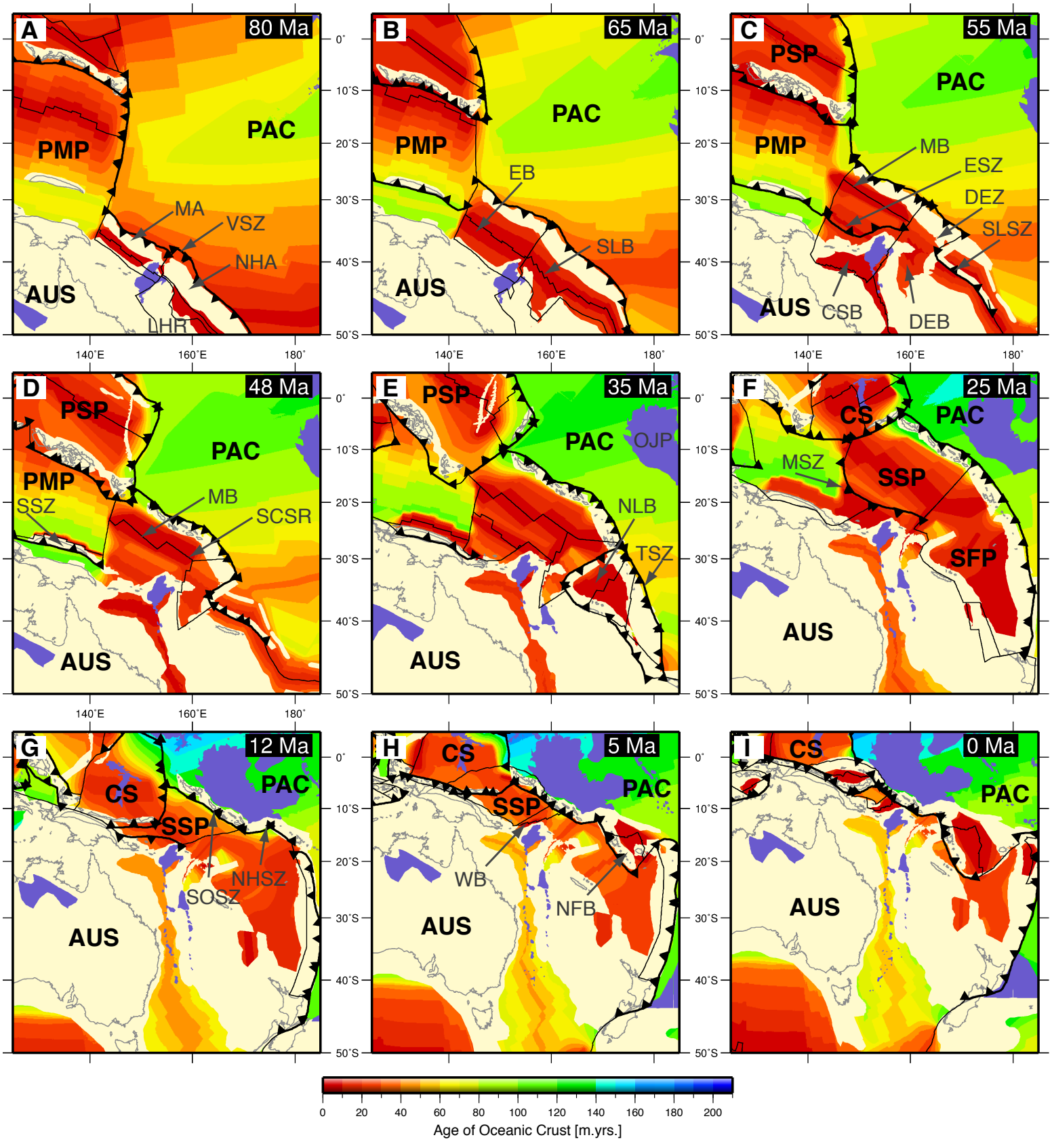

Seton et. al. Fig. 14

Table1

Table 1. Summary of dredge localities, rock types and analyses

Dredge	Location	Lat (°S)	Long (°E)	Depth (m)	Approx. wt (kg)	Rocks (excl. Mn nodules	Ar-Ar & geochem	Micropal-entology	Spinels
DR1	Louisiade Plateau, SE side	13.2012	157.9813	3000-3500	30	Pale brown soft mudstone		Y	
DR2	Rennell Ridge, SW side	12.2042	159.7074	2800-3500	150	Cream-grey calc-mudstones, some sandy		Y	Y
DR3	Rennell Ridge, NE side	12.0251	160.8317	2200-2800	50	Basalts, some jointed and pillowed, with rare lst-cemented volcanic breccia	Y	Y	
DR4	West Torres Plateau, W tip	13.8801	163.3189	2600-2900	50	Basalt, some with glassy rinds	Y	Y	Y
DR5	East Lapérouse Rise, NE end	13.6510	162.2192	1200-1600	300	Cream-coloured varitextured limestones		Y	
DR6	East Lapérouse Rise, mid part	14.4534	161.1168	2600-3000	1	Basalt	Y		Y
DR13	South Rennell Trough, W scarp	16.6396	158.8356	1530-2000	3	Pale cream-coloured limestone		Y	
DR14	South Rennell Trough, E scarp	17.0755	159.1991	2600-3200	400	Basalt lavas and associated volcanic breccia, sandstone and mudstone	Y		Y

Table2

Table 2. Summary of Ar-Ar dating

Dredge	Site	GNS #	UCSB #	Material	wt. (mg)	TFA (Ma)	WMPA (Ma)	ISOA (Ma)	% gas	K/Ca	J	Pref. age
DR3Ai	Rennell Ridge, NE side	P82182	SB66-7,8,10,11	Plagioclase	25.9	45.8±0.8	42.3±1.2	42.5±15	32	0.001-0.003	0.0041962	42.0 ± 2.0
DR3Aiv	Rennell Ridge, N side	P82183	SB66-13,14	Plagioclase	14.1	45.5±0.8	43.2±1.0	42.8±2.2	57	0.004-0.007	0.0041830	43.2 ± 1.5
DR4Bi	West Torres Plateau	P82189	SB66-15	Plagioclase	21.1	25.2±0.8	26.2±0.8	25.5±5.0	69	0.005-0.030	0.0041784	26.2 ± 0.8
DR6A	East Lapérouse Rise	P82193	SB66-43	Plagioclase	25.6	39.9±0.6	39.3±0.6	39.1±1.2	92	0.002-0.005	0.0041987	39.3 ± 1.2
DR14Eiii	South Rennell Trough	P82206	SB66-45	Groundmass	26.7	30.8±0.4	30.1±0.5	30.8±1.6	28	0.003-0.970	0.0041991	30.0 ± 2.0
DR14G	South Rennell Trough	P82217	SB66-51	Plagioclase	23.9	34.8±0.4	34.7±0.4	34.3±1.2	79	0.005-0.006	0.0041887	34.7 ± 0.5

GNS#=Institute of Geological and Nuclear Sciences Petrology Collection number, UCSB#=University of California Santa Barbara irradiation number, TFA=total fusion age, WMPA=weighted mean plateau age, ISOA=inverse isochron age, J=dimensionless irradiation parameter, Pref. age= preferred interpreted age.

e-component: supplementary material

Click here to download e-component: Seton++_Supplementary_Material_Summary_revision_unmarked.docx

Supplementary Figure 1

Click here to download e-component: SupplFig1_Seton++.pdf

Supplementary Figure 2

Click here to download e-component: SupplFig2_Seton++.pdf

Supplementary Figure 3

Click here to download e-component: SupplFig3_Seton++.pdf

e-component: supplementary Figure 4

Click here to download e-component: SupplFig4_Seton++_NEW.pdf

e-component: supplementary Figure 5

Click here to download e-component: SupplFig5_Seton++_NEW.pdf

Supplementary File A

Click here to download Raw research data (under CC BY license; see above): SupplFileA_Seton++.pdf

Supplementary File B

Click here to download Raw research data (under CC BY license; see above): SupplFileB_Seton++.pdf

Supplementary File C

Click here to download Raw research data (under CC BY license; see above): SuppFileC_Seton++.pdf

Supplementary File D

Click here to download Raw research data (under CC BY license; see above): SupplFileD_Seton++.pdf

e-component: animation - Plate_Reconstruction_Animation_Seton++.mov

This file could not be included in the PDF because the file type is not supported.

Data directory

Click here to download Raw research data (under CC BY license; see above): Seton++_Data.zip